Article

Novel Meta-Fractal Wearable Sensors and Antennas for Medical, Communication, 5G, and IoT Applications

Albert Sabban

Department of Electrical Engineering, ORT Braude College, Karmiel 2161002, Israel; sabban@braude.ac.il; Tel./Fax: +972-4-875-9111

Abstract: Future communication, 5G, medical, and IoT systems need compact, green, efficient wideband sensors, and antennas. Novel linear and dual-polarized antennas for 5G, 6G, medical devices, Internet of Things (IoT) systems, and healthcare monitoring sensors are presented in this paper. One of the major goals in the evaluation of medical, 5G, and smart wireless communication devices is the development of efficient, compact, low-cost antennas and sensors. Moreover, passive and active sensors may be self-powered by connecting an energy-harvesting unit to the antenna to collect electromagnetic radiation and charge the wearable sensor battery. Wearable sensors and antennas can be employed in smart grid applications that provide communication between neighbors, localized management, bidirectional power transfer, and effective demand response. A low-cost wearable antenna may be developed by etching the printed feed and matching the network on the same substrate in the printed antenna. Active modules may be placed on the same dielectric board. The antenna design parameters and a comparison between the computation and measured electrical performance of the antennas are presented in this paper. The electrical characteristics of the new compact antennas in the vicinity of the patient's body were simulated by using electromagnetic simulation techniques. Fractal and metamaterial efficient antennas and sensors were evaluated to maximize the electrical characteristics of smart communication and medical devices. The dual- and circularly polarized antennas developed in this paper are crucial to the evaluation of wideband and multiband compact 5G, 6G, and IoT advanced systems. The new efficient sensors and antennas maximize the system's dynamic range and electrical characteristics. The new efficient wearable antennas and sensors are compact, wideband, and low-cost. The operating resonant frequency of the metamaterial antennas with circular split-ring resonators (CSRRs) may be 5% to 9% lower than the resonant frequency of the sensor without CSRRs. The directivity and gain of the metamaterial fractal antennas with CSRRs may be up to 3 dB higher than the antennas without CSRRs. The directivity and gain of the metamaterial fractal passive sensors with CSRRs may be up to 8.5 dBi. This study presents new wideband active meta-fractal antennas and sensors. The bandwidth of the new sensors is around 9% to 20%. At 2.83 GHz, the receiving active sensor gain is 13.5 dB and drops to 8 dB at 3.2 GHz. The receiving module noise figure with TAV541 LNA is around 1dB.

Keywords: 5G and 6G devices; active sensors; energy harvesting; green sensors; fractal antennas; IoT; medical applications; metamaterial antenna; smart grid sensors; wearable antennas

1. Introduction

Printed compact antennas and sensors are widely used in wearable communications, IoT, and monitoring healthcare systems. Low efficiency and narrow bandwidth are the major disadvantages of printed small antennas, as presented in [1–4]. Compact, efficient wideband wearable antennas, such as printed dipole, loop, slot, patch, fractal, and FIPA antennas, are presented in [2–5]. The theory of metamaterial antennas with periodic structures has been discussed and presented in books and journals (see [2–6]). Materials with periodic artificial structures are known as metamaterials. The artificial material structure

and the periodic resonant elements characterize the electrical and mechanical specifications of the metamaterial. In [7–11], periodic structures and metallic posts, such as periodic circular split-ring resonators (CSRRs), are used to produce materials with a required dielectric constant value and permeability. Metamaterial technology can be used to evaluate compact, wideband, low-cost wearable antennas for wireless RF devices, 5G and 6G, medical sensors, healthcare monitoring sensors, and other wearable devices [12–16]. The gain and bandwidth of the metamaterial microstrip antenna presented in [6] are like those of conventional patches. In [8], metamaterial structures with negative permittivity are developed and presented. In [9], the authors analyze and measure the polarity of SRR structures. A transmission-line antenna with metamaterial segments is discussed in [12]. Compact, wideband, efficient passive and active metamaterial sensors and antennas for RF systems, cellular phones, IoT, and healthcare systems are discussed in [15–19]. In [2,3,18], measurement setups and measured results of antennas in the vicinity of the user's body are discussed and provided. Fractal antennas are used in many RF devices and systems. A fractal antenna uses an antenna design with several similar fractal elements to increase and maximize the radiator-effective area. Fractal antennas may be defined as having multilevel geometry with space-filling curves. Usually, fractal radiators are small, wideband, multiband, and employed in wireless communication and RF systems. Fractal radiators have been analyzed and evaluated in journals, books, and patents [20–25]. Several wearable and fractal antennas and sensors are analyzed and presented in [22–32]. Small antennas are analyzed and presented in [33]. Wearable medical sensors and devices are employed to monitor patients to improve disease cures and prevent disease spread. A hospital IoT-based management platform used to monitor patients' health is presented in [34]. Wearable wideband sensors and antennas for smart grid SG, healthcare, and communication applications are discussed in [35–43]. Wearable medical devices may be used to monitor and test a patient's daily health [34,35]. In [40], dual-polarized wearable radiators for wearable healthcare devices and for RF systems are discussed. Compact wideband novel metamaterials and fractal antennas for energy-harvesting systems are presented in [44–57].

In this work, fractal and metamaterial technology is employed to evaluate compact, wideband, efficient antennas and sensors for 5G, 6G, and IoT, healthcare, and communication systems. Meta-fractal antennas and sensors have not been presented in major publications in the last decade. The receiving active antenna gain is 13.5 dB at 2.83 GHz and decreases to 8 dB at 3.2 GHz, and the receiving module noise figure with TAV541 LNA is around 1 dB. The new efficient meta-fractal sensors and antennas maximize the system's dynamic range and electrical characteristics. The sensors and antenna types discussed in this paper and their advantages are summarized in Table 1.

Table 1. Features of antennas and sensors presented in this paper.

Antenna Type	Gain dB	BW %	Effic. %	Beamwidth		Optimized Parameters	Application	Polarization
				θE ⁰	θH⁰			
Stacked Fractal	7.8	8	91	76	78	Fractal shapes, layer spacing	Medical, 5G, IoT, SG	Linear
Meta-Fractal	8	20	90	76	90	Fractal shapes, CSRR size	Medical, 5G, IoT, SG	Linear
Stacked Meta-Fractal	8.5	14	95	72	80	Fractal shapes, CSRR size	Medical, 5G, IoT, SG	Linear
Circular Meta-Fractal	8	12	90	74	74	Fractal shapes, CSRR size	Medical, 5G, IoT, SG	Dual band
Active Rx. Meta-Fractal	13	50	90	74	74	Fractal shapes, CSRR size	Medical, 5G, IoT, SG	Dual band

2. Wearable Technologies Status in 2023

In 2023, wearable devices became extremely popular, and this helped users collect, monitor, and analyze real-time personal information. Wearable devices are worn by people to monitor, evaluate, and transmit individuals' data and can save users' lives. Wearable devices can monitor medical data from the heartbeat rate, temperature, sleep behaviors, and sweat.

2.1. Benefits of Wearable Devices and Technology

- Physicians have a fast response to evaluate and diagnose patient health. The healthcare treatment process is faster due to the information acquired by the worn sensors.
- Athletes can improve their fitness and training process thanks to the healthcare information collected by worn sensors and antennas.
- Equipping workers with wearable sensors improves the health and productivity of the workers.
- Wearable sensors and antennas improve communication between workers, monitor staff activity, improve companies' safety measures, and may improve the productivity rate of employees, life quality, and the health of the users. These facts save companies up to millions of dollars annually.
- Wearable sensors and devices are employed to monitor IoT networks and devices.
- Hospital daily activities such as patient healthcare, patient sleep patterns, monitoring the heartbeat, blood pressure, and patient temperature may be monitored by wearable sensors and antennas.
- By employing wearable sensors and IoT devices to automate companies' daily work, companies' hardware and labor costs may be reduced.

2.2. Wearable Technology Applications and Examples, [49–52]

Medical wearables. Wearable medical sensors, and wearable medical devices are employed to track daily hospital activities such as patient healthcare, patient sleep patterns, monitoring the heartbeat, blood pressure, sugar rates, and patient temperature. Wearable devices are worn by individuals to track, monitor, and transmit personal health data. These medical devices can monitor healthcare information from the heartbeat rate, temperature, sleep behaviors, and sweat.

Education Wearables. Smart glasses and virtual reality (VR) headsets allow universities and companies to train students and workers by using simulations and virtual environments. Users are faced with real-life situations that allow them to spend more time learning and practicing real-life situations. Moreover, headbands and brain sensors monitor and track when a person's brain is stressed and when it is relaxed. Education organizations can use these sensors to learn when students are stressing their minds too much and educate them on how to remain calm and relaxed.

Epidermal skin technology. The Terasaki Institute for Biomedical Innovation invented wearable electronic skin for monitoring health. This ultra-thin e-skin patch can be attached to the user's chest zone with a compact wireless transmitter. The sensor picks up and records electro signals, such as muscle movements, which can be sent to medical centers via the internet and the cloud so they may track the daily user's health information. This worn sensor may track chronic illnesses such as epilepsy, diabetes, and heart illnesses.

Health monitoring. Individuals employ worn sensors to monitor and track information about their health condition, heartbeat, sweat, user temperature, and blood pressure and examine their calorie budget. The 2019 COVID pandemic increased the growth of the wearable devices market as people care more about their private healthcare and monitor the spread of infections.

Wearable Gaming industry. Gaming companies and entertainment organizations were among the first to use smart glasses, controllers, and VR headsets in the gaming industry. VR headset displays, such as Sony PlayStation, VR Meta Quest, Oculus Quest, and others, are employed in many gaming smart devices, virtual traveling, movie entertainment, gaming machines, and entertainment devices.

Fashion and smart clothing. Smart dressing and clothing became popular in the last decade. Smart shirts and jackets are composed of electrical fibers that allow the user to receive phone calls and listen to entertainment programs and music. The user may use a built-in camera to take videos or photos right from their smart clothing. Smartwatches, smart jewelry, smart shoes, and wristbands are examples of popular wearable technology that is in continuous growth.

Wearable military devices. Wearable military devices include devices and sensors that track soldiers. Boot inserts can estimate how well the soldiers are holding their equipment. Wearable sensors can monitor and test soldiers' performance and health in several conditions and climates and how terrain factors can affect soldiers' performance**.**

Sports and fitness. Amateur and professional athletes use wearable athletic sensors and devices that are part of the sport equipment, such as, hats, shoes, bats, and balls. Wearable sports sensors can be built into the fabric of sports apparel. The Bluetooth-linked devices and GPS devices provide real-time information to coaches to monitor and analyze the athlete's health performance. The progress in the development of wearable antennae in the last thirty years is given in Table 2.

Table 2. Progress in the development of compact wearable antenna characteristics, 1993–2023.

Antennas Type	1993–2011 [3]			2012–2023 [2]		
	Gain dB	BW%	Effic. %	Gain dB	BW%	Effic. %
Printed dipoles	3	5	70	4	5	80
Patches	3.5	5	70	4	5	80
Stacked patches	7	12	85	7.5	15	85
Metamaterial Ant.	4	10	50	8–8.5	50	92
Metamaterial Antenna with strips	-	-	-	5–8	50	92
Fractal Antennas	4.5	5	70	5	10	82

3. Design Consideration of Compact Antennas and Sensors for Wearable Devices

Fractal and metamaterial antennas may be employed in multiservice and multiband advanced systems. The major advantage of the new meta-fractal antenna lies in the wideband and multiband efficient performance of the antenna network. Multiband compact antennas are crucial in multiband communication systems. This results in the easy connection of a small, low-cost printed radiator for wideband and multiband RF communication networks, medical systems, IoT, and cellular phones. The major features and advantages of the new meta-fractal antennas are that they have similar characteristics (input impedance, gain, and radiation pattern) at multiband frequencies with similar electrical characteristics and are better than traditional antennas such as dipole and slot antennas. Fractal and metamaterial antennas have smaller dimensions compared to other traditional antennas. The new advanced antennas provide better flexibility to develop multiband antennas for commercial and military platforms, devices, and systems. Fractal antennas are compact, efficient, wideband, and multiband and may be used in wireless RF systems, as well as IoT, medical, and communications systems. Fractal structures are presented in Figure 1. Metamaterials are artificial materials with periodic metallic and dielectric structures. The material structure and the periodic resonant elements define the electrical and mechanical characteristics of the metamaterial. Metallic segments and periodic rectangular or circular split-ring resonators (CSRRs) may be used to produce materials with a

designed dielectric constant and permeability that cannot be achieved by conventional materials. Printing SRRs or CSRRs on the radiating elements reduces the antenna size and may result in a wideband, compact, efficient antenna. The theory of metamaterial antennas and fractal antennas is presented in several papers and books. The metamaterials, see [9–16], antennas and fractals, see [20–24], and antennas developed and presented in this paper were evaluated by using electromagnetic ADS Momentum software [44]. The wearable small passive and active antennas and sensors are multiband, flexible, efficient, and low-cost. The resonant frequency of the metamaterial antennas with CSRRs is lower by 5% to 9% than the resonant frequency of antennae without CSRRs. The directivity and gain of the metamaterial antennas with CSRRs are higher by 2 dB to 3 dB than the antennas without CSRRs. The directivity and gain of the new passive antennas with CSRRs are around 7.8dBi. The new meta-fractal advanced antenna bandwidth is around 9% to 20%. The bandwidth of the antennas presented in Sections 6 to 8 is around 9% to 20%.

    (**a**)   (**b**)   (**c**)   (**d**)
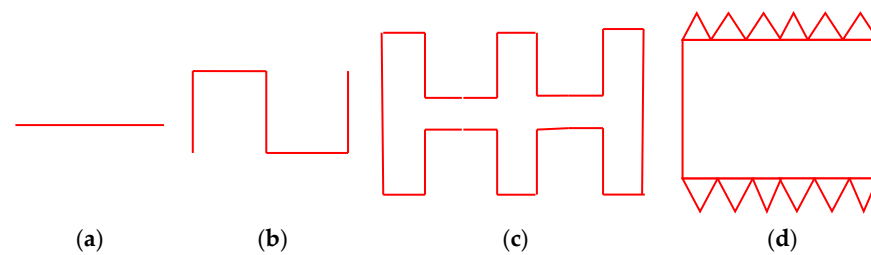
Figure 1. Fractal segments: (**a**) line, (**b**) bended line, (**c**) bended line fractal structures, and (**d**) fractal structure.

Design Considerations and Challenges in Development of Compact Antennas

Most conventional antennas, such as dipole, loop, and slot antennas, are Euclidean antennas. In conventional antennas, the antenna-radiating area is directly proportional to the radiator dimensions. In conventional antennas, when the length of the square is doubled, the actual area of the antenna is increased by a factor of four. Electrical characteristics of conventional antennas (such as the gain, impedance, and efficiency) are the function of the antenna's size-to-wavelength ratio. Small conventional antennas are typically narrowband antennas. Small antennas with a size much smaller than the RF system wavelength, (λ), become very inefficient because the antenna's radiation resistance, R_r, is lower than R_c, the ohmic resistance. In this case, the antenna does not couple electromagnetic real power to free space, the antenna stores reactive power within its near field area (reactive impedance Xc). Conventional small antennas have a high quality factor, Q, and a lower bandwidth. Q may be defined as the ratio of input reactance Xin to radiation resistance Rr, $Q = {X_{in}}/{R_r}$. The quality factor is inversely proportional to the bandwidth. Radiation resistance R_r of a circular loop-shaped antenna is written in Equation (1).

$$R_r = 20\pi^2({C}/{\lambda}) \tag{1}$$

The loop perimeter is C. The resistance R_c for C < 1 is greater than the radiation resistance R_r, and the antenna is highly inefficient. A small antenna will have a relatively large ohmic resistance and a relatively small radiation resistance. Radiation resistance Rr of a fractal antenna decreases as a small power of the perimeter (C). A fractal loop has a higher radiation resistance than a small Euclidean loop antenna of equal size. Fractal antennas are antennas that use an antenna design with similar fractal segments to maximize the antenna's effective area. Fractal and metamaterial antenna geometry can be used to overcome the limitation of small Euclidean antennas. A metamaterial antenna functions as if it were much larger than its actual size because its novel structure stores and re-radiates energy. Artificial metamaterial periodic structures and periodic resonant elements, such as SRRs, characterize the electrical and mechanical specifications of the metamaterial. Periodic structures and metallic posts, such as periodic circular split-ring resonators

(CSRRs), are used to produce materials with the required dielectric constant value and permeability. The metamaterial structure can be designed and optimized to develop efficient compact antennas. Figure 1a–d present several fractal segments.

4. Green Stacked 2.5 GHz Fractal Wearable Antenna with an Energy-Harvesting Unit

The stacked fractal fabricated patch antenna is shown in Figure 2a,b. The resonant first layer was etched on a dielectric substrate, duroid 5880, with a 2.2 dielectric constant and 0.8 mm thickness. A fractal square patch is etched on the second layer. The fractal patch was etched on an FR4 substrate with a 4.5 dielectric constant and 0.8 mm thickness. The electromagnetic energy radiated by the resonator is coupled to the fractal patch antenna. The patch radiator dimensions are 45.2 × 48.8 × 0.08 mm. The spacing between the two layers can be varied to increase the antenna bandwidth. For a VSWR better than 2:1, the antenna bandwidth is 5% for an air spacing of 10 mm between the two layers. The antenna center frequency is 2.6 GHz. For a VSWR better than 2.5:1, the antenna bandwidth is 8% for an air spacing of 8 mm between the two layers. The antenna computed and measured gain is around 7.8 dBi, the antenna E plane beamwidth is 76°, and the antenna H plane beamwidth is around 76°. The antenna efficiency is 91%. As shown in Figure 2c, the energy-harvesting unit is connected to the antenna and consists of a rectifying circuit and a rechargeable battery.

(**a**)

(**b**)

(**c**)

(**d**)

(**e**)
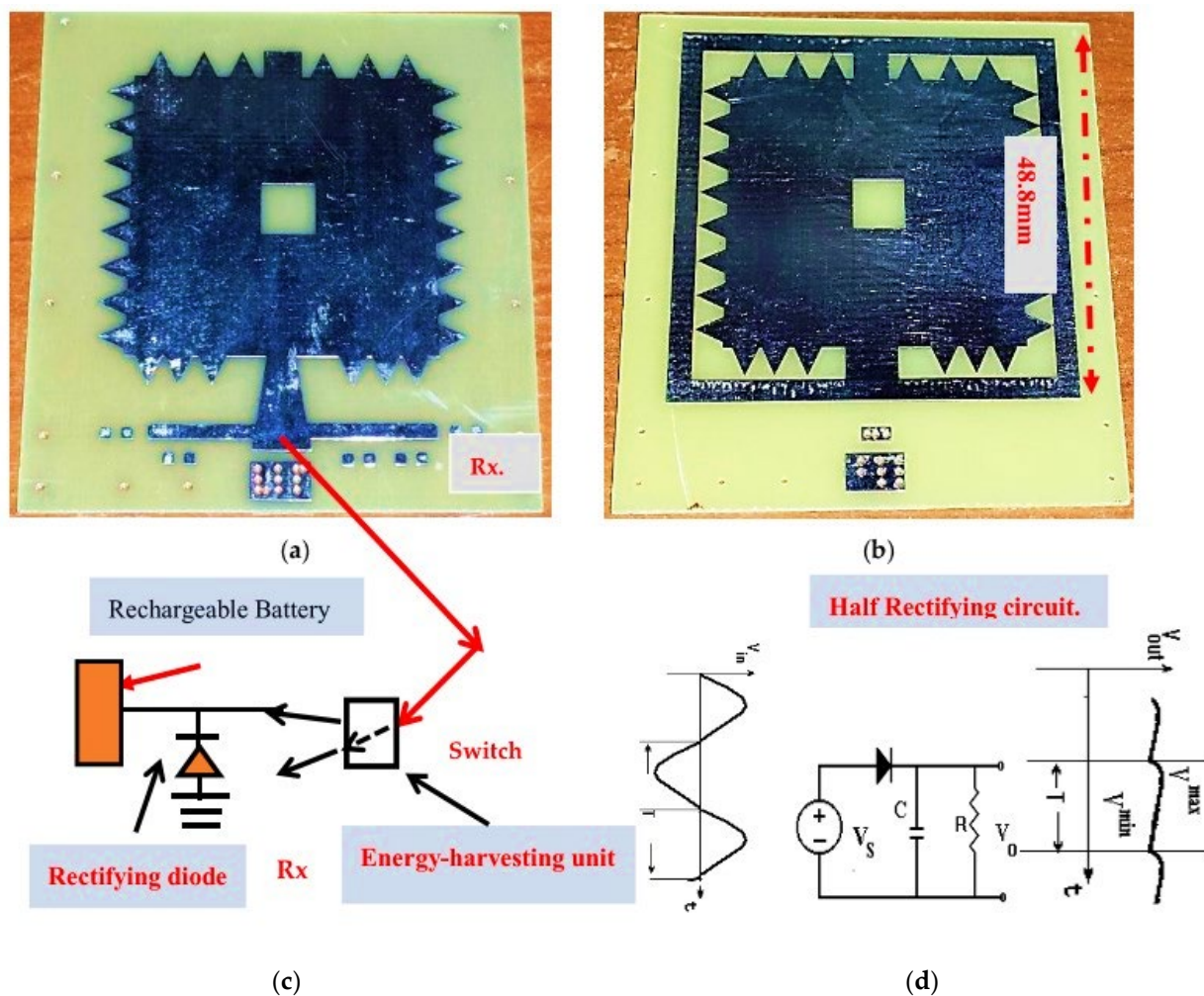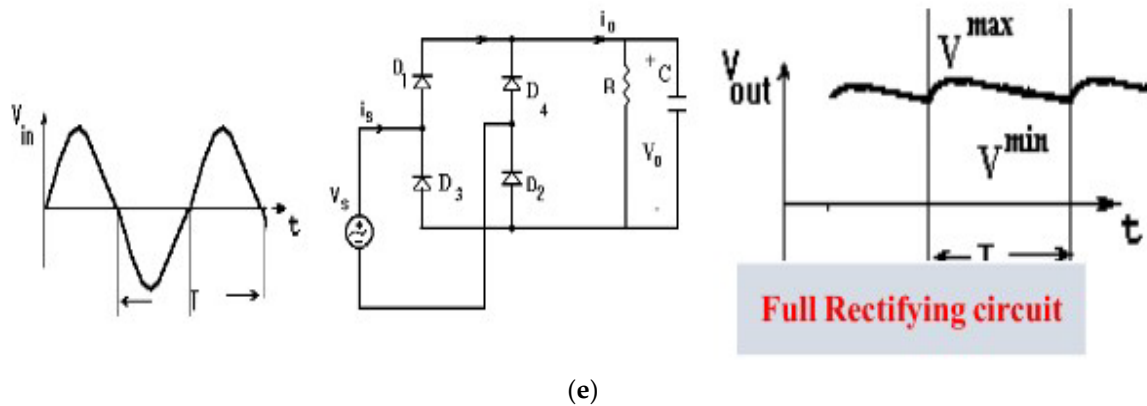
Figure 2. (**a**) Fabricated stacked patch, first layer—resonator. (**b**) Second layer—radiator. (**c**) Energy-harvesting unit. (**d**) Diode voltage half-wave rectifier with a capacitor. (**e**) Full-wave rectifier.

The energy-harvesting unit and the antenna provide a self-powered sensor. The rectifier diode converts RF energy, AC energy, to direct current (DC energy). Usually, two types of diode rectifiers are used: a half-wave or a full-wave rectifier [45–49]. V_{ODC} is the rectifier output voltage and is written in Equation (2). The rectifier output voltage can be flattened and improved by adding a capacitor in shunt to the resistor, as written in Equation (3). The capacitor works as a low-pass filter to flatten the output DC voltage.

$$V_{O,DC} = \frac{1}{2\pi} \int_0^{2\pi} V_O^{MAX} \sin(\omega t)\, d(\omega t); \quad \omega = 2\pi f$$

(2)

$$V_O = V_S - V_{DON} \approx V_S; \quad V_O{}^{MAX} = V_m$$

$$V_{ODC} = V_m/\pi$$

$$Vripple = Vr = Vmax - Vmin = {VDC}/{fCR}$$

(3)

The time constant τ should be lower than T. Where $\tau = RC \ll T$. Equation (4) verifies that the half-wave rectifier efficiency is 40.6%. The RF diode resistance is negligible as compared to R. A half-wave rectifier is presented in Figure 2d. The half-wave rectifier converts only the positive voltage half-cycle.

$$\eta = \frac{\text{DC output power}}{\text{AC input power}} = \frac{\left(\frac{Im}{\pi}\right)^2 R}{\left(\frac{Im}{2}\right)^2 (R+rf)} \sim 0.406$$

(4)

A full-wave bridge rectifier is presented in Figure 2e. The bridge rectifier consists of four diodes. During the positive half-cycle voltage, terminal A will be positive and terminal B will be negative. Diodes D1 and D2 will become forward biased and D3 and D4 will be reversed biased. Equation (5) verifies that the full-wave rectifier efficiency is 81.2%. A Schottky diode can be used as a rectifier diode.

$$\eta = \frac{\text{DC output power}}{\text{AC input power}} = \frac{\left(\frac{2Im}{\pi}\right)^2 R}{\left(\frac{Im}{2}\right)^2 (R+rf)} \sim 0.812$$

(5)

Schottky diodes are semiconductor diodes that have a low forward voltage drop and a very fast switching action. There is a small voltage drop across the diode terminals when current flows through the diode. The voltage drop of a Schottky diode is usually between 0.15 and 0.5 volts. This lower voltage drop provides better system efficiency and a higher switching speed. A normal diode has a voltage drop between 0.6 to 1.7 volts. One of the Skyworks Schottky diodes from the SMS-7630 series may be chosen because of their

ultralow capacitance, low forward voltage, low series resistance, and fast switching response. Schottky diode SMS-7630-061 was employed in this research as the rectifying diode.

Energy-harvesting units can be connected to the sensors presented in this paper to provide green, renewable energy, and can eliminate the usage of power cords and the need to replace batteries frequently. In Figure 3, S11 parameters of the fractal-stacked patch with 10 mm air spacing are presented. The radiation pattern of a fractal-stacked patch is presented in Figure 4a,b. The measured gain is plotted on the computed results to present the agreement between these results. This new compact, efficient fractal antenna can maximize the dynamic range and electrical characteristics of RF, 5G, IoT, and medical systems.
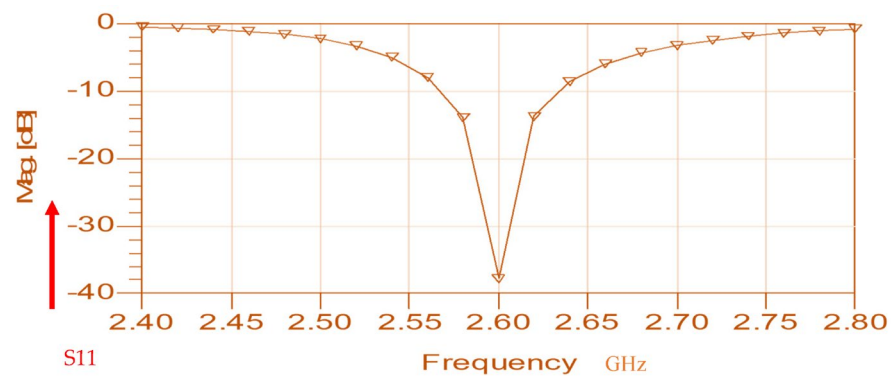
Figure 3. S11 parameter of the wearable fractal-stacked patch antenna.

(**a**)

(**b**)
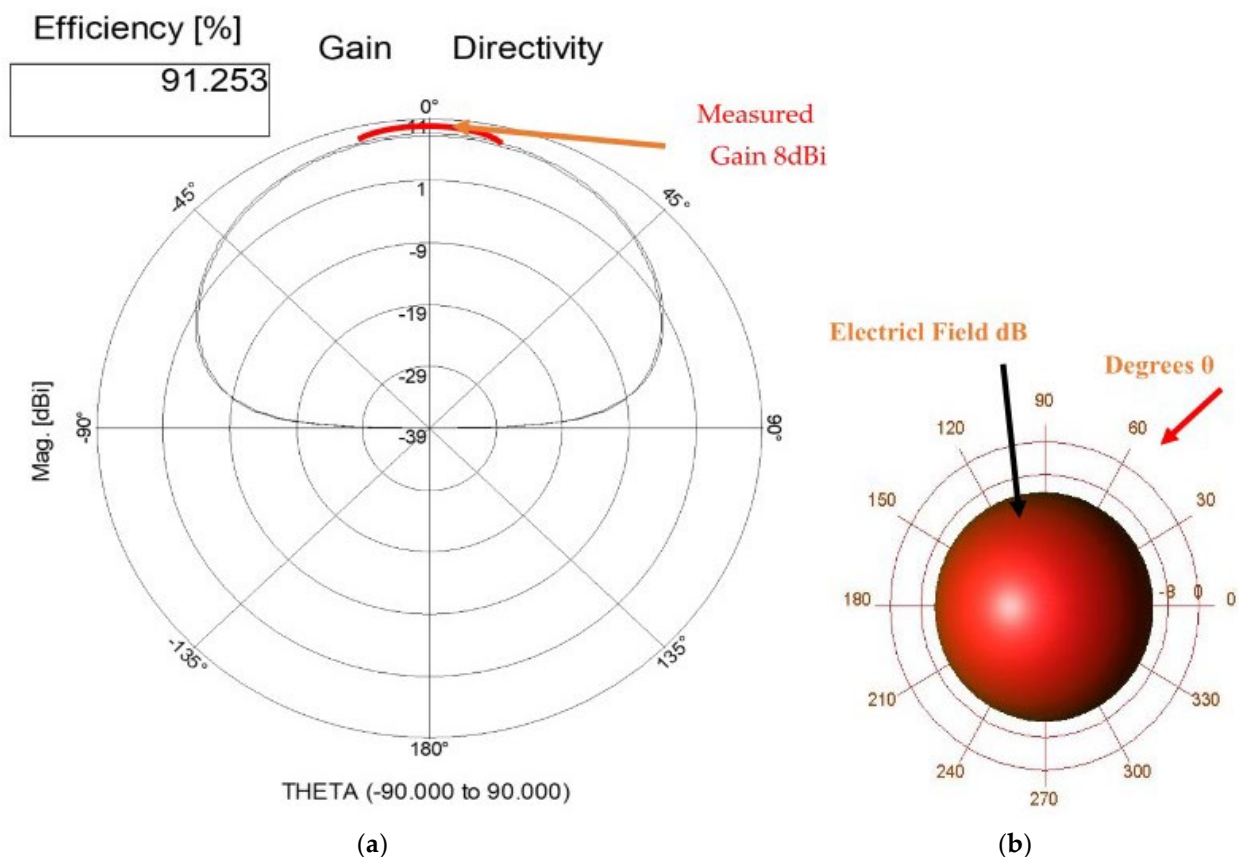
Figure 4. (**a**) Wearable fractal-stacked patch antenna radiation pattern at 2.6 GHz. (**b**) Three-dimensional radiation pattern.

5. Compact Metamaterial Fractal Wearable Antenna

A dual-band compact meta-fractal wearable antenna is shown in Figure 5. The fractal patch was etched on a dielectric substrate with a 2.2 dielectric constant and 3.2 mm thickness. Ten CSRRs are printed on the rectangular microstrip antenna. The rectangular fractal patch size is 35 × 19 mm. The outer diameter of the CSSR is 5.2 mm. The width of a rectangular patch without CSSRs and fractal segments should be 23.33 mm. By using CSSRs and fractal segments, the antenna width is shorter by almost 20%. Matching stubs are etched on the fractal antenna feed line. The antenna structure and matching network are optimized to design a dual-band antenna. The resonant frequencies are 4.5 GHz and 5.5 GHz; see Figure 6. The measured and computed fractal patch gain is around 8 dBi. The 3D antenna radiation pattern is presented in Figure 7a,b. The antenna E and H beamwidths are around 78° and 90°, respectively.
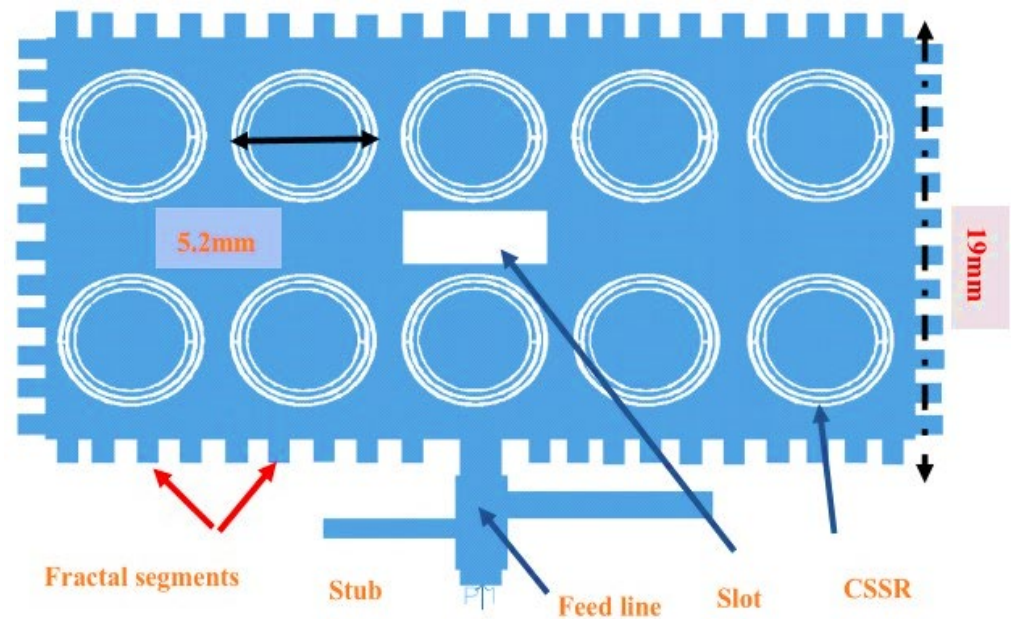
Figure 5. A compact metamaterial fractal wearable antenna.
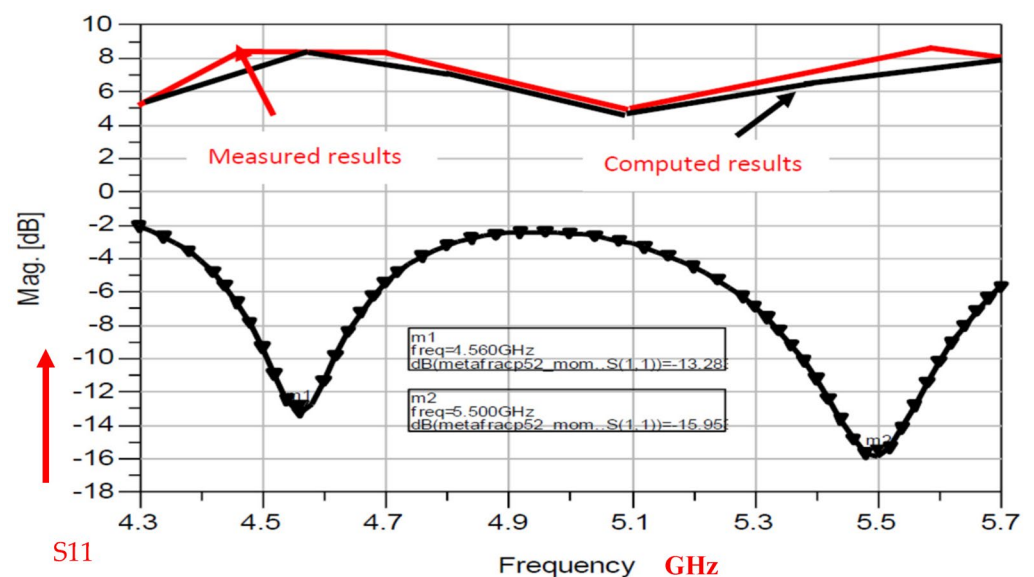
Figure 6. S11 parameter of the dual-band wearable metamaterial fractal antenna.
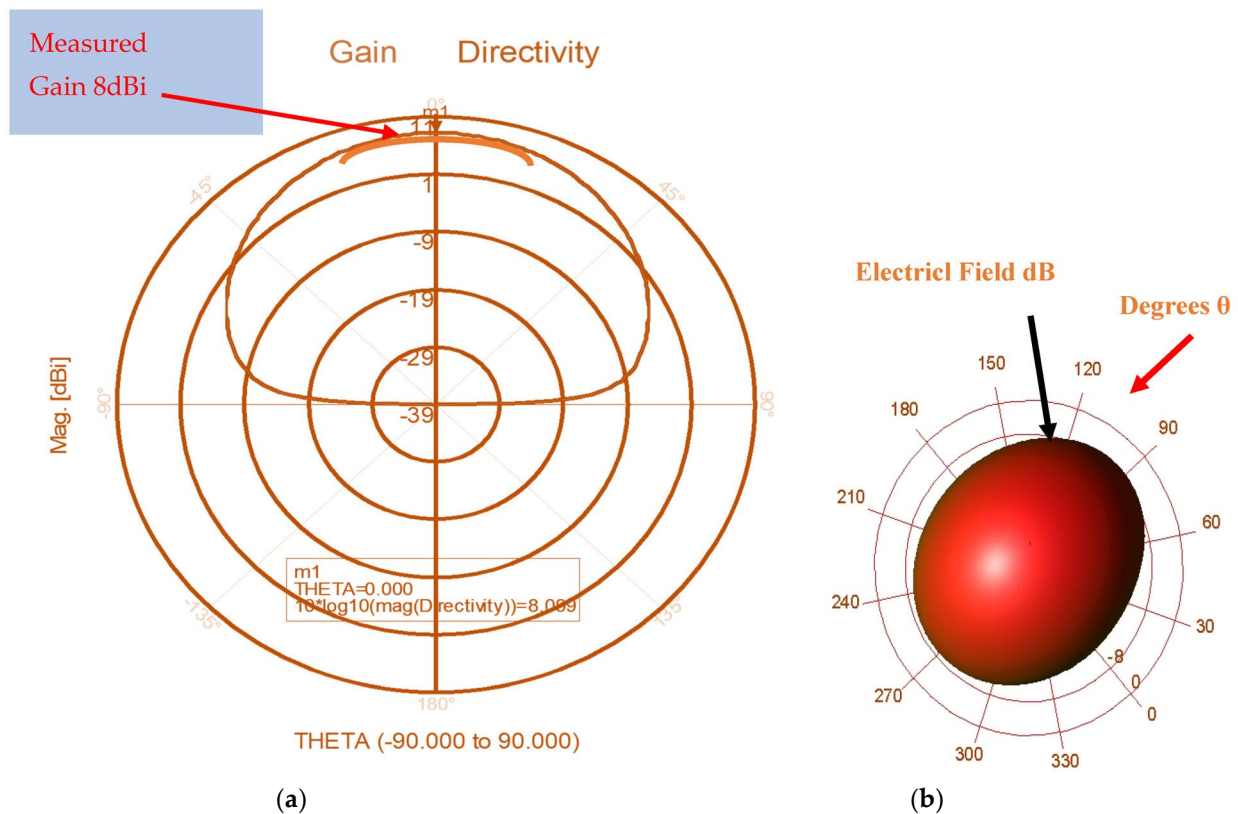
Figure 7. (**a**) Wearable dual-band meta-fractal antenna radiation pattern at 4.6 GHz. (**b**) The 3D radiation pattern.

The discrepancy between the computed and measured gain presented in Figure 6 is around 0.5 dB. Usually, the accuracy of an antenna's gain measurement is around ±0.4 dB. The VSWR of the measurement cable setup may affect the measured gain results. We may conclude that there is a good match between the simulation and measured S11 and the gain of the antenna.

6. Compact Double Layers Wideband Wearable Metamaterial Sensor

A wideband, compact, stacked meta-fractal antenna is presented in Figure 8. The stacked meta-fractal antenna has ten CSRRs printed on the radiator. The fractal segments are printed on the resonator. The antenna has two layers separated by air spacing. The resonator is printed on the first FR4 layer with a dielectric constant of 4 and is 1.6 mm thick. The radiator is printed on the second layer with a dielectric constant of 2.2 and is 1.6 mm thick. The size of the meta-fractal antenna presented in Figure 8 is 33 × 20 × 3.2 mm. The meta-fractal antenna was developed and optimized by simulating ADS RF electromagnetic, W3601B, software [44]. The small size of the antennas presented in this paper allows them to be attached to the human body. The antennas have conformal features. The fractal metamaterial antennas presented in this paper are compact, with dimensions less than 0.55λ, and they can be used as radiating elements in antenna arrays.

The width of the antenna without CSSRs and fractal segments should be 28 mm. By using CSSRs and fractal segments, the antenna width is shorter by almost 25%. Matching stubs are connected to the antenna's feed line. The antenna structure and feed network were optimized to increase the antenna's bandwidth and efficiency. For a VSWR better than 2:1, the antenna bandwidth is 14%. The antenna's E and H beam widths are around 76° and 80°, respectively, with 7 to 8 dBi gain. There is a good match between the simulation and measured S11 and the gain of the antenna. The antenna efficiency is around 95%.

The simulated S11 is presented in Figure 9. The radiation pattern of the stacked meta-fractal antenna is shown in Figure 10.
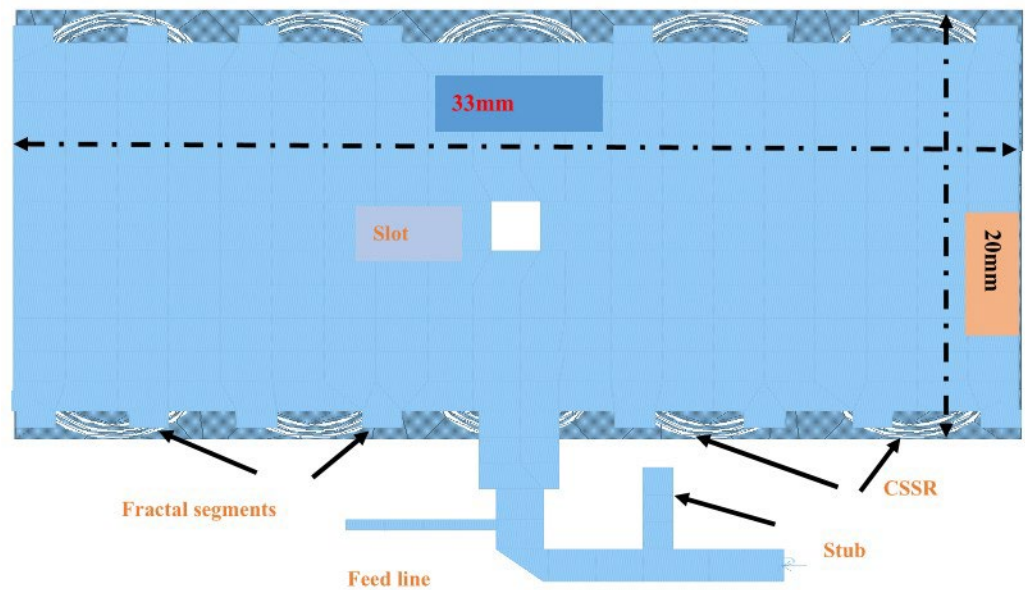
Figure 8. Wearable metamaterial fractal-stacked patch antenna.
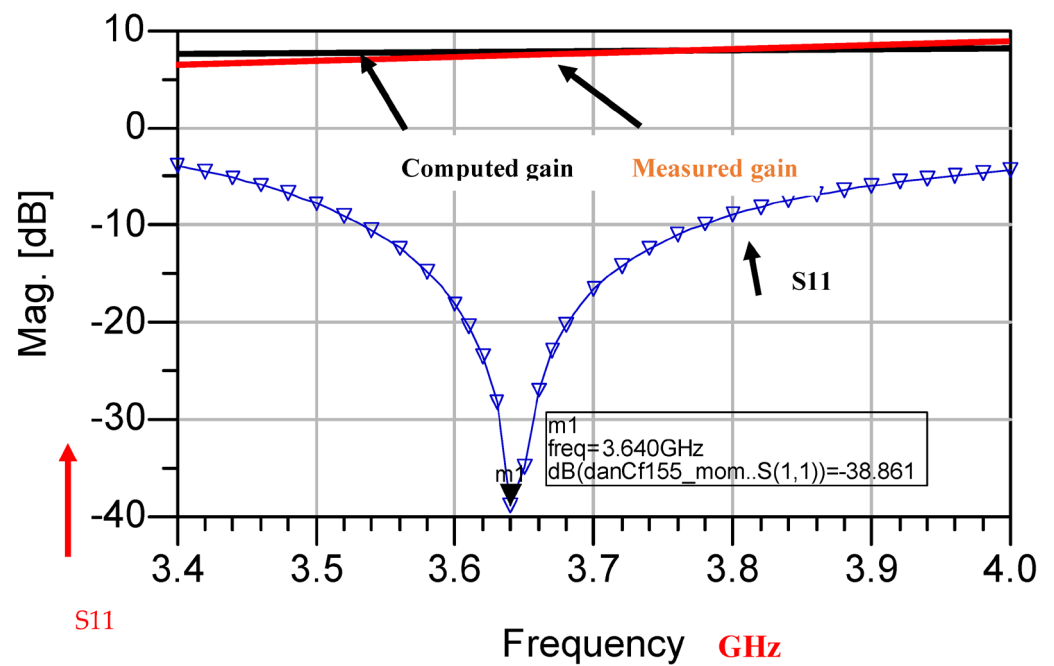
Figure 9. Wearable stacked metamaterial fractal patch antenna S11 parameter.
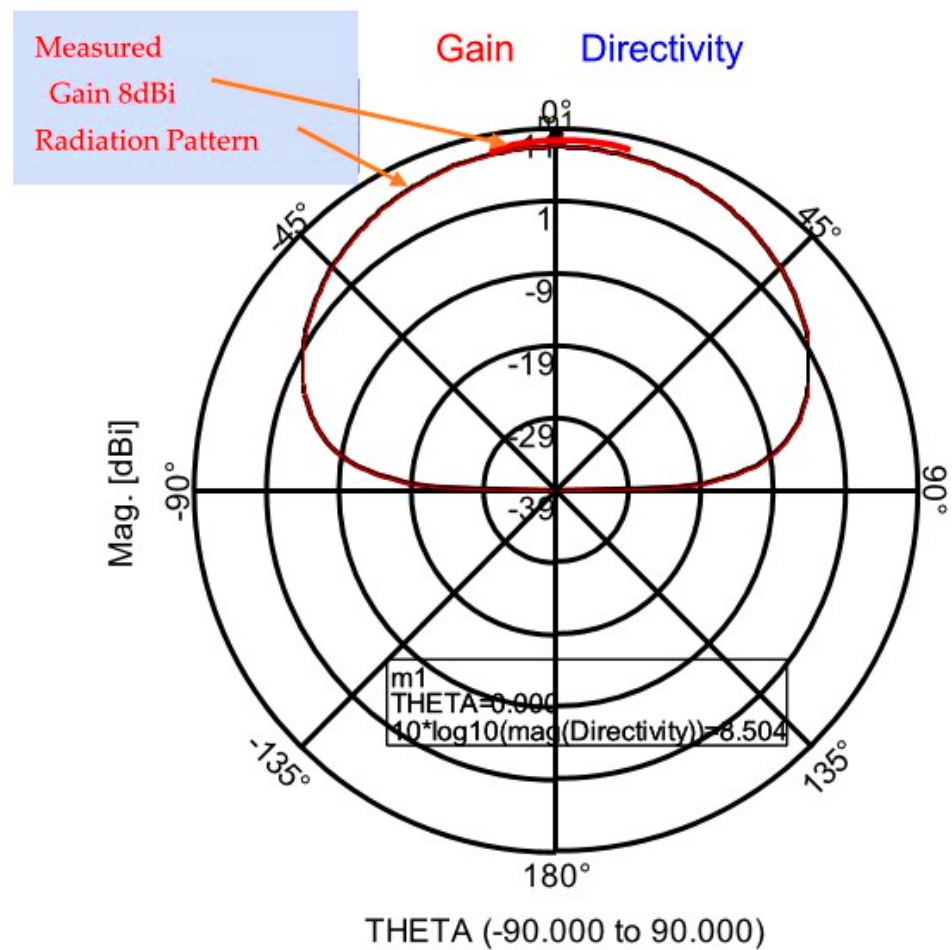
Figure 10. Directivity and gain at 3.6 GHz of the stacked metamaterial fractal antenna with SRR.

7. Green Dual-Polarized Wearable Metamaterial Fractal-Stacked Circular Antenna

A meta-fractal-stacked circular patch with CSRRs and the coordinate system are shown in Figure 11a,b. The antenna consists of two layers. The circular resonator with eighteen CSSRs and fractal segments is printed on a substrate with a dielectric constant of 2.2 and is 1.6 mm thick, with a loss tangent of 0.002. The circular patch antenna with fractal segments is shown in Figure 11c. The radius of the circular patch with fractal segments is 20.5 mm. The diameter of the circular resonator with CSSRs is 39 mm. The antenna's center frequency is 2.8 GHz. The resonant frequency of the dominant mode TM11 of the circular patch may be computed by using Equation (6) [1]. The light velocity in a vacuum is c. Where $2a_e$ is the diameter of the circular patch and may be computed by using Equation (7), ε_e is the effective dielectric constant. At 2.8 GHz, the radius of the circular patch should be 22.2 mm. The radius of the outer CSRR ring is 2.6 mm, as presented in Figure 11a and in the CSSR photo in Figure 11d.

$$f = \frac{1.8412c}{2\pi a_e \sqrt{\varepsilon_e}} \tag{6}$$

$$a_e = \frac{1.8412c}{2\pi f \sqrt{\varepsilon_e}} \tag{7}$$
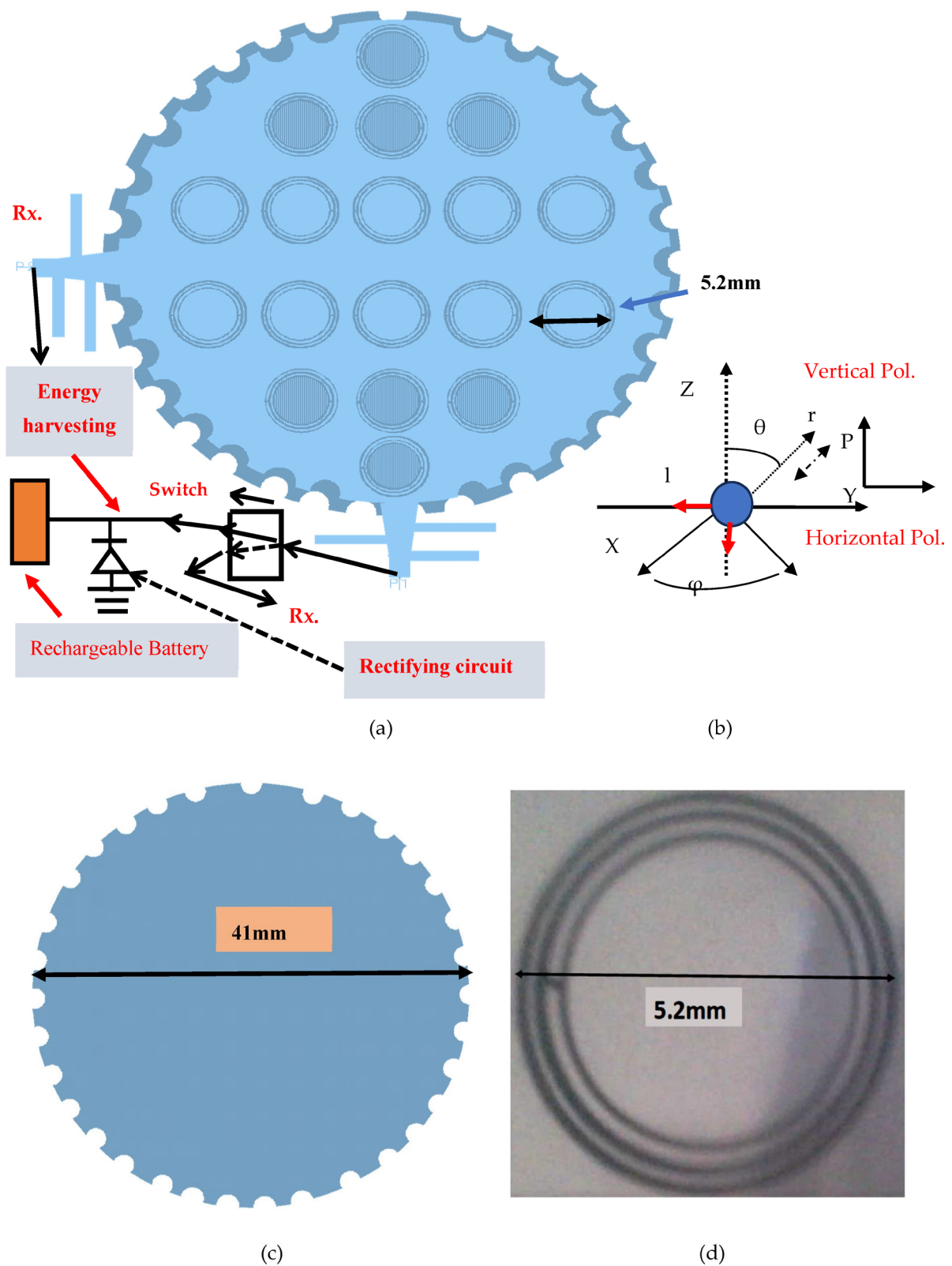
Figure 11. (**a**) Metamaterial fractal dual-polarized circular wearable antenna with energy-harvesting unit. (**b**) Coordinate system. (**c**) Fractal radiator. (**d**) Fabricated CSRR photo.

The CSRR strip's width is 0.15 mm. The antennas and CSRRs developed in this paper were designed and optimized by using 3D electromagnetic software [44]. The radius of the circular patch without CSRR is greater by 13% than the radius of the circular antenna

with CSRR. In [2–5,16], the theory and design details of the CSRRs are given. As shown in Figure 11a, energy-harvesting units are connected to the antenna's horizontal and vertical ports. The circular patch antenna's bandwidth is around 12% for S11, lower than −6 dB; see Figure 12. The horizontal and vertical antenna gain is around 8 dBi; see Figure 12.

The antenna E and H beam width is around 74°, as shown in Figure 13a. The directivity and gain of the circular meta-fractal antenna are higher by 2.5 dB to 3 dB than a circular stacked patch without CSRR. By increasing the air spacing between the resonator and the radiator, the antenna bandwidth may be increased. The microstrip antenna's bandwidth is the function of the antenna thickness and is higher for thicker microstrip antennas [2–4]. The antenna's 3D radiation pattern is presented in Figure 13b. The measured results are plotted on the simulation results to illustrate the agreement between the computed and measured results; see Figures 4, 6, 7, 9, and 10. In Figure 10, the computed efficiency is 100%, and the measured efficiency is around 95% due to losses in the feed network.
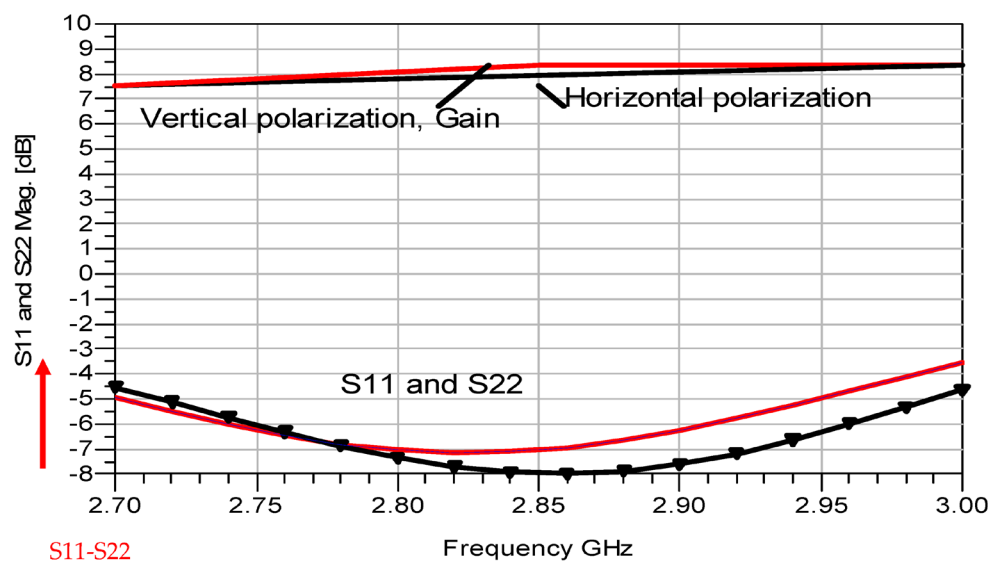
Figure 12. Gain and S11 and S22 parameters of the stacked meta-fractal wearable antenna.
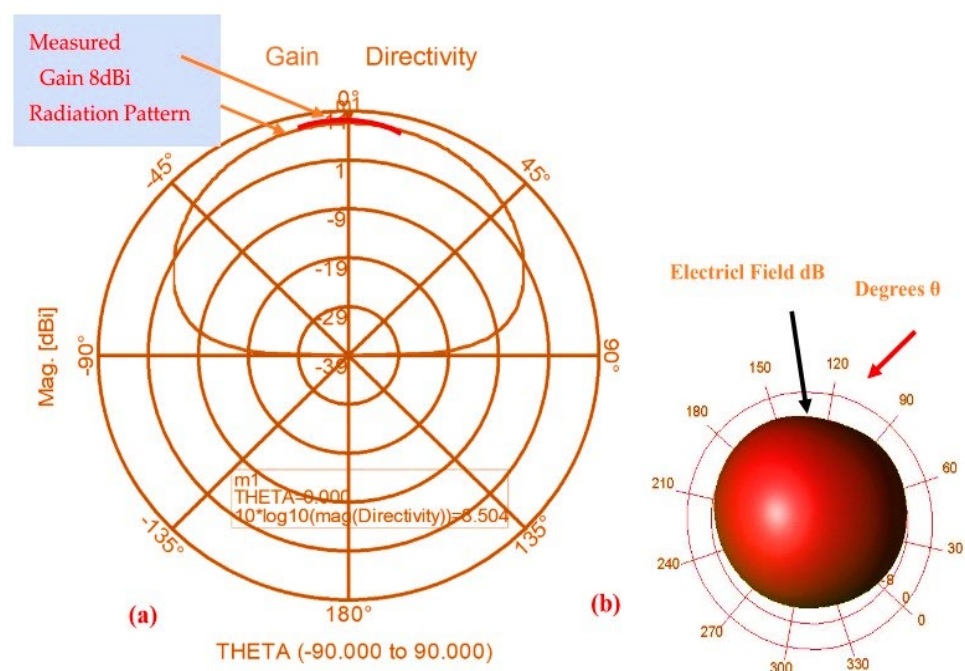
Figure 13. (**a**) Gain of the circular stacked meta-fractal antenna at 2.8 GHz. (**b**) The 3D radiation pattern.

8. New Active Receiving Dual-Polarized Stacked Circular Wearable Antenna

A low-noise amplifier, LNA, was attached to the circular meta-fractal patch antenna shown in Figure 11 and presented in Section 7. The active receiving antenna configuration is shown in Figure 14. The Mini-Circuits TAV541 PHEMT LNA is connected to the antenna feed line via a printed input-matching circuit that matches the antenna to the LNA. A printed output-matching circuit matches the LNA output to the receiver. The size of the printed input- and output-matching circuits is around 20 × 30 mm. A DC unit provides the required bias voltages to the LNAs. Table 3 presents the amplifier characteristics. In Table 4, the LNA S parameters are given. The active antenna noise figure, with the LNA TAV541, is around 1 dB for frequencies from 0.5 GHz to 3 GHz. The active antenna gain is 13.5 dB at 2.83 GHz and drops to 8 dB at 3.2 GHz. The circular patch antenna S11 parameter on a patient's body is presented in Figure 12. Figure 15a presents the S21 and S12, measured and calculated, of the horizontal polarization of the active receiving dual-polarized meta-fractal wearable antenna. Figure 15b presents the S21 and S12 of the vertical polarization of the active receiving dual-polarized meta-fractal wearable antenna. The horizontal and vertical gain, S21, of the active antenna is around 20 dB at 0.5 GHz and 10 dB at 2.5 GHz. The isolation, S12, is lower than −30 dB. The S11 and S22 of the antenna are better than −6 dB from 1 GHz to 3 GHz. For a VSWR better than 2:1, the antenna bandwidth is around 25%. The results presented in Figure 15 indicate that the receiving antenna with the TAV541 is better in frequencies from 0.5 GHz to 1.5 GHz. By replacing the LNA TAV541 with the analog device's PHEMT amplifier HMC459, the active antenna is higher, 12 ± 2 dB in frequencies from 0.8 GHz to 3 GHz, as presented in Figure 16. The matching circuit of the circular-polarized receiving antenna with VNA25 is shown in Figure 17. The matching network consists of matching stubs and microstrip matching transmission lines. The HMC459 specifications are presented in Table 5. However, the active antenna noise figure is around 4 dB. The active antenna power consumption with HMC459 is 2.3 W. The active antenna power consumption with the LNA's TAV541 is 0.3 W. The dual-polarized antenna can function as a circularly polarized antenna by connecting a 3 dB 90° coupler to the vertical and horizontal ports of the antenna, as presented in Figure 18. The circular-polarized meta-fractal antenna bandwidth is around 17% for VSWR, better than 2:1 in frequencies from 2.5 GHz to 3 GHz. The circular-polarized meta-fractal circular patch gain is 7.8 dBi with around a 76° beam width. There is a good match between the simulation and measured results.
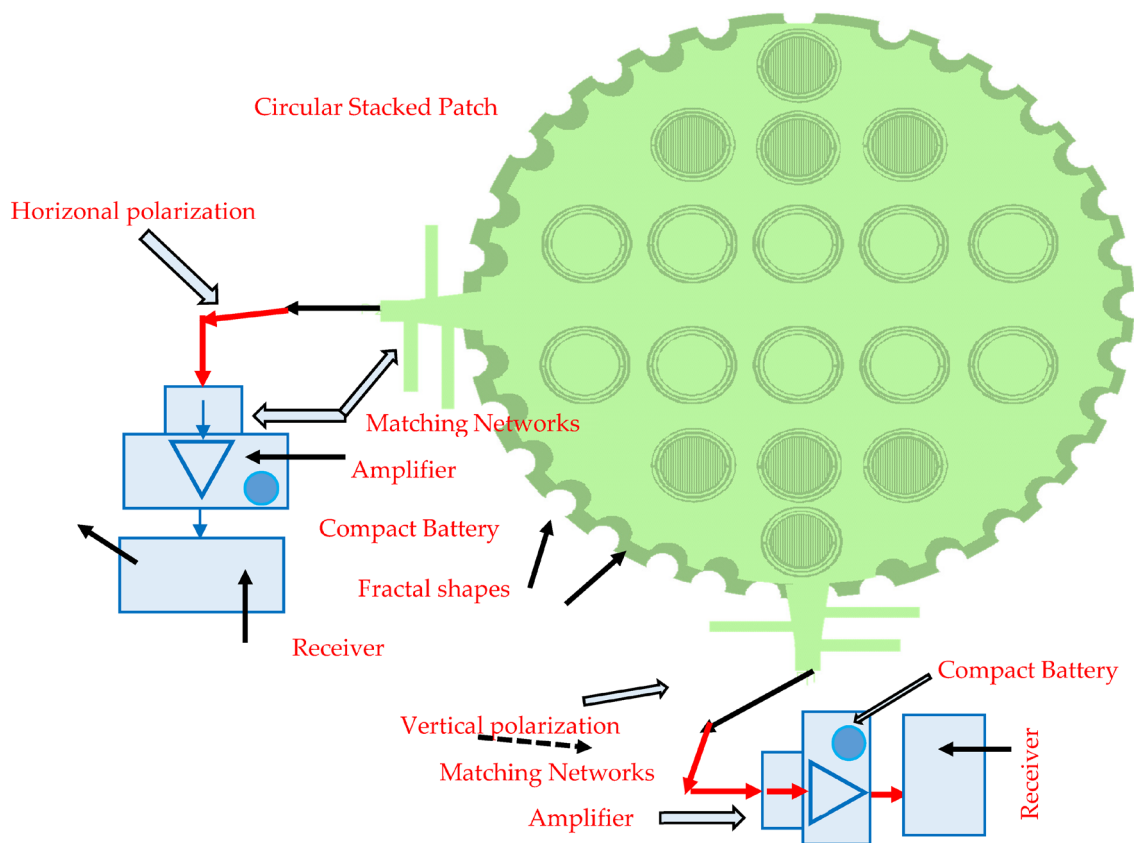
Figure 14. Active receiving dual-polarized meta-fractal-stacked circular wearable antenna.
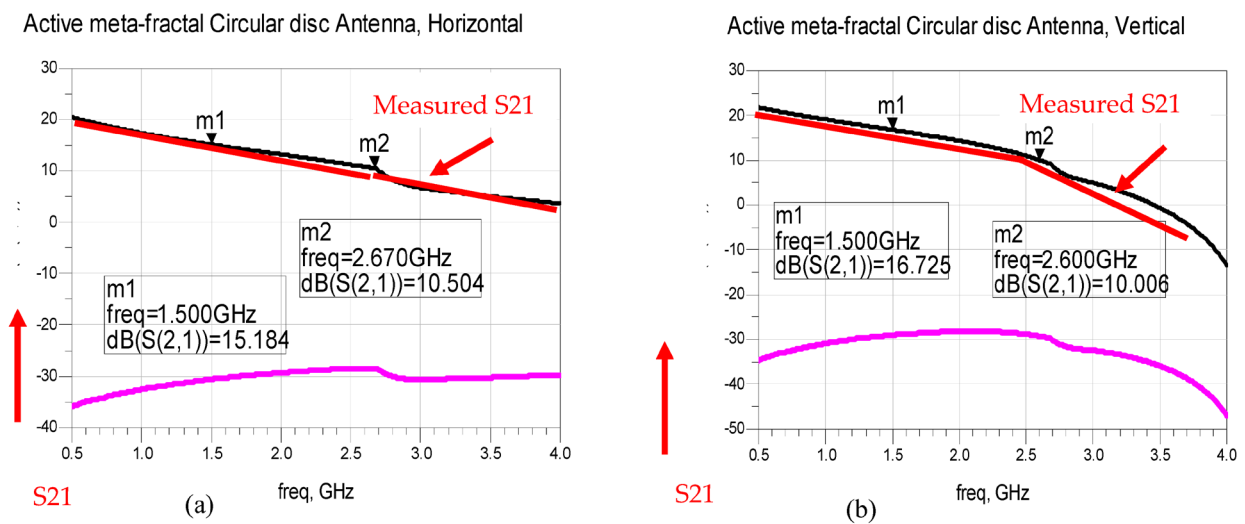
Figure 15. (**a**) S21 and S12 of the horizontal polarization of active receiving dual-polarized meta-fractal wearable antenna. (**b**) S21 and S12 of the vertical polarization of active receiving dual-polarized meta-fractal wearable antenna.
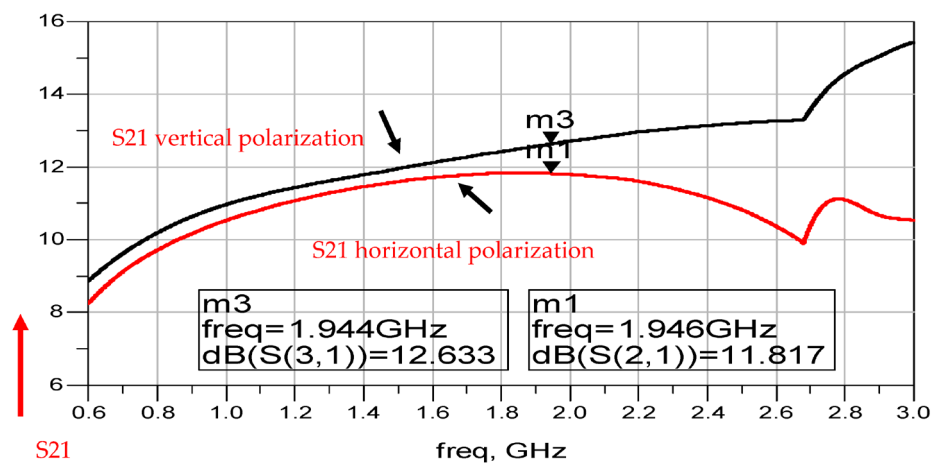
Figure 16. S21 of the active receiving dual-polarized meta-fractal wearable antenna.
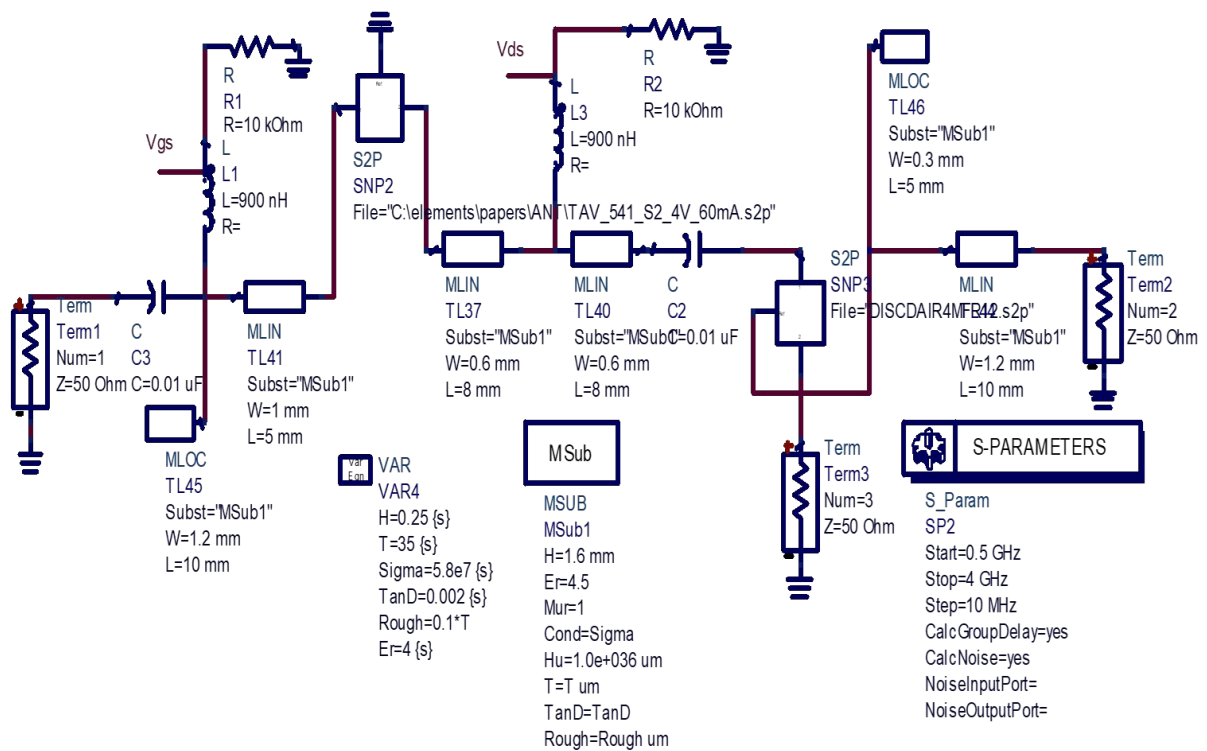
Figure 17. Matching circuit of the circular-polarized receiving antenna with TAV541.
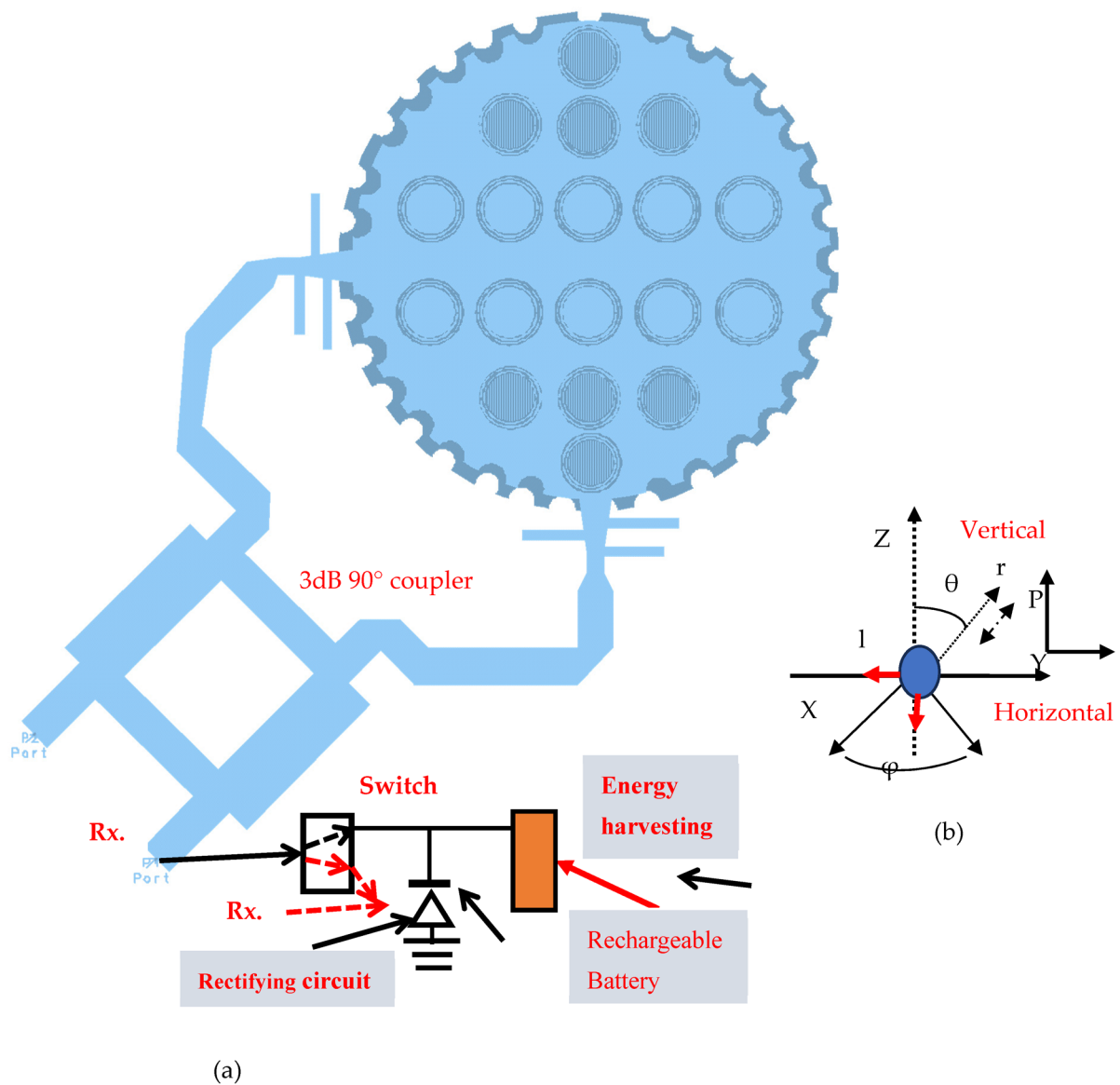
Figure 18. (**a**). Green circular-polarized metamaterial fractal wearable antenna. (**b**) Coordinate system.

Table 3. Electrical characteristics of the LNA, TAV541.

Parameter	Specification	Remarks
Frequency	0.4–3 GHz	-
Gain at 2 GHz	17.9 dB	Vds = 3 V
N.F at 3 GHz	0.8 dB	-
P1 dB at 3 GHz	19.5 dBm	-
OIP3 at 2 GHz	33 dBm	-
Max input power	17 dBm	-
Vgs	0.50 V	-
Vds	3 V	Ids = 60 mA
Supply voltage	±5 V	-
Package	Surface Mount	-
Operating temperature	−40 °C–80 °C	-

Table 4. LNA S parameters, TAV541.

F-GHz	S11	S11°	S21	S21°	S12	S12°	S22	S22°
0.10	0.99	−17.17	25.43	168.9	0.008	88.22	0.55	−14.38
0.28	0.93	−45.77	22.97	149.5	0.021	65.77	0.51	−33.65
0.41	0.89	−65.72	20.98	137.27	0.03	57.9	0.46	−49.3
0.50	0.87	−77.1	19.54	130.3	0.034	53.03	0.43	−57.5
0.73	0.80	−100.8	16.22	115.7	0.042	42.06	0.36	−74.86
0.82	0.77	−108.8	15.07	110.75	0.044	39.53	0.34	−80.87
1.04	0.74	−126.2	12.74	100.13	0.05	33.69	0.29	−94.96
1.21	0.71	−137.6	11.25	92.91	0.051	30.05	0.26	−104
1.53	0.69	−154.2	9.30	82.06	0.055	26.08	0.22	−119
1.75	0.67	−164.1	8.24	75.31	0.06	23.14	0.20	−128.4
2.02	0.67	−174.6	7.30	67.82	0.06	20.88	0.18	−138.8

Table 5. Specification of HMC459 MMIC Amplifier.

Parameter	Specification	Remarks
Frequency	DC–18 GHz	-
Gain at DC to 6 GHz	18 dB	Vds = 8 V
N.F at DC to 6 GHz	4 dB	-
P1dB DC to 6 GHz	24 dBm	-
OIP3 at DC to 6 GHz	34 dBm	-
Max input power	17 dBm	-
Vgs	0.50 V	-
Vds	3 V	Ids = 290 mA
Supply voltage	±5 V	-
Operating temperature	−55 °C–85 °C	-

Energy-harvesting units can be connected to the antenna's horizontal and vertical ports, as presented in Figure 11. Theory and detailed information about energy-harvesting systems is presented in [45–49]. A comparison between the printed wearable metamaterial antennas with and without CSRR is listed in Table 6.

Table 6. Comparison between printed wearable antennas with and without CSRR.

Antenna	Frequency (GHz)	BW %	BW% Measured	Computed Gain dBi	Measured Gain dBi	Length. (cm)	Efficiency %
Meta-fractal-stacked	3.45–3.9	16	15	8	8.3	2	95
Meta-fractal-stacked circular patch	2.7–2.9	11	10	8	8.2	4.1	95
Meta circular-polarized patch	2.4–2.8	15	14	8.3	8	3.6	90
Meta circular	2.5–2.7	9	9	7.5	7.8	3.6	85
Circular patch without CSRR [2,3]	2.6–2.65	1.5	1.5	4.5	4.3	4.8	85
Printed dipole with CSRR [2,3]	0.32–0.36	11	10	5.6	5.7	19.8	95
Dipole without CSRR [2,3]	0.38–0.42	10	12	2.5	2.5	21	90
Meta-stacked circular patch	2.6–2.8	9	10	8.5	8.4	4	95
Stacked circular patch	2.6–2.8	8	8	5.4	5.3	4.8	89

9. Wearable Sensors and Antennas for Medical, 5G, 6G, Smart Grid, and IoT Applications

The meta-fractal antennas and sensors developed in this paper may be used in medical, IoT, 5G, 6G, smart grid, and communication applications. The antennas and sensors' reflection coefficient variation near the user's body was computed by using the patient's body and sensors model presented in Figure 19a,b. The dielectric constant, conductivity, and attenuation of human body tissues are given in Table 7. The antenna's electrical characteristics near the patient's body are evaluated by computing the antenna's reflection coefficient near the human body. The dielectric constant of the body tissues varies from 5 in fat tissues to 38 in the lung tissues and to 128 in the small intestine tissues. The dielectric constant and conductivity of the body tissues may be employed to compute the attenuation α of RF transmission through human tissues, as given in Equations (8) and (9). The attenuation of electromagnetic waves of heart and colon tissues at 0.6 GHz is 20 dB/m.

Table 7. Attenuation and electrical characteristics of human body tissues [26,27].

Tissue	Parameter	440 MHz	600 MHz	1 GHz	1.25 GHz
Heart/Colon tissues	σ	1.00	1.05	1.32	1.46
	ε	63.52	61.95	60.00	59.45
	Attenuation, dB/m	18	20	24	27
Fat tissues	σ	0.047	0.05	0.054	0.06
	ε	5.00	5.00	4.72	4.55
	Attenuation, dB/m	3.5	3.9	4.5	4.8
Stomach tissues	σ	0.70	0.76	0.97	0.99
	ε	42.7	41.40	39.1	39.00
	Attenuation, dB/m	16	18	22	25
Blood	σ	1.76	1.78	1.91	1.99
	ε	57.2	56.5	55.40	55.00
	Attenuation, dB/m	38	40.8	46.34	49.3
Skin	σ	0.58	0.6	0.63	0.77
	ε	41.6	40.45	40.25	39.65
	Attenuation, dB/m	14	15.3	18	19
Lung tissues	σ	0.27	0.27	0.27	0.28
	ε	38.4	38.4	38.4	38.4
Kidney tissues	σ	0.90	0.90	0.90	0.91
	ε	117.5	117.5	117.5	117.5
Prostate	σ	0.75	0.75	0.90	1.05
	ε	50.5	50.0	46.7	46.5
	Attenuation, dB/m	16.5	18.5	22.5	25
Small intestine	σ	1.74	1.74	1.74	1.74
	ε	128.1	128.1	128.1	128.1
	Attenuation, dB/m	27	28	28.7	29
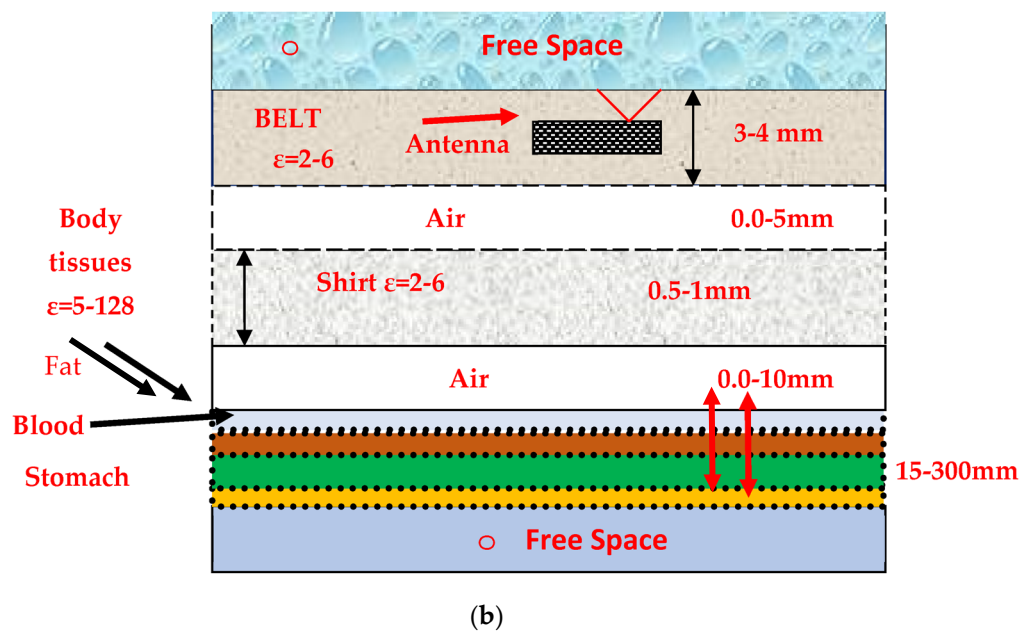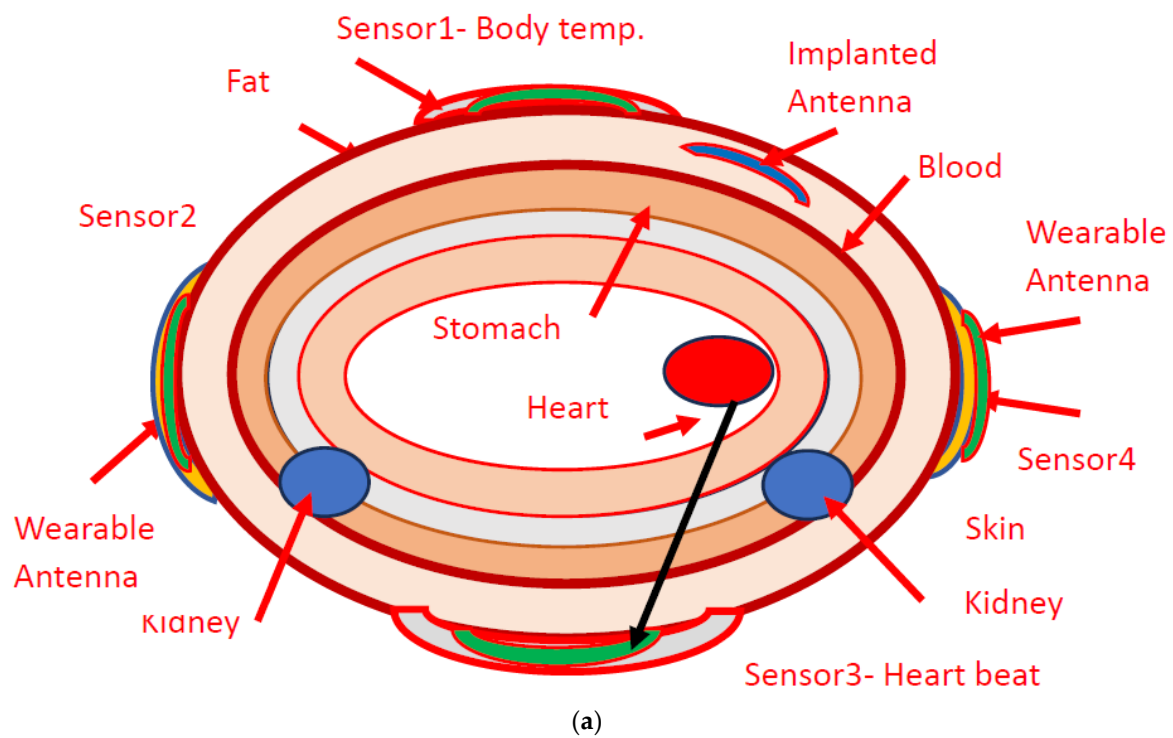
Figure 19. (**a**) Healthcare application of wearable antennas. (**b**) Analysis model of wearable antennas.

The electrical features of the body tissues change the antenna's resonant frequency up to 6% at different positions of the sensor on the human body. The antennas may be placed inside a belt, as presented in Figure 20. The belt's electrical features may change the antenna's resonant frequency.
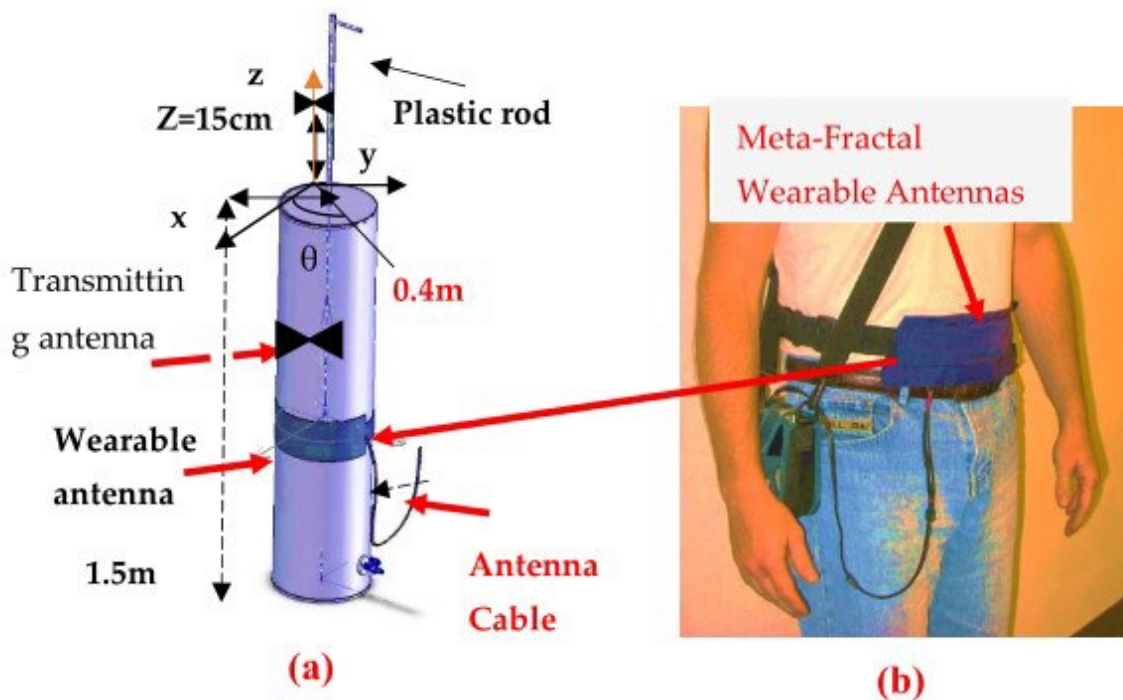
Figure 20. (**a**) Phantom configuration. (**b**) Photo of the meta-fractal antenna inside a belt.

The electrical and mechanical parameters were optimized to develop a compact sensor with the best electrical and mechanical characteristics. The wearable sensors' electrical characteristics were simulated and measured for air spacing between the sensors and the user's body up to 10 mm at different positions on the user's body. The radiation performance of wearable sensors is measured by employing a phantom. The phantom can be used to measure the radiation characteristics from inside or outside the phantom. The phantom contains a mix of water, sugar, and salt that represents human body tissues' electrical characteristics. The relative amount of water, sugar, and salt determines the electrical features of the phantom environment. A mixture of 55% water, 44% sugar, and 1% salt presents the electrical characteristics of stomach tissues. The length of the phantom fiberglass cylinder is 1.5 m with a radius of 0.2 m and a thickness of 2.5 mm, as presented in Figure 20a. The phantom contains a plastic rod that is 5 mm thick. The position of the plastic rod may be adjusted and rotated inside the phantom. A compact transmitting antenna can be placed on the plastic rod at different heights. We can rotate the antenna in the x–y plane. A photo of the meta-fractal antenna inside a belt is shown in Figure 20b. Energy-harvesting circuits can be connected to the meta-fractal antennas and sensors presented in this paper.

The phantom mixture affects the wearable antenna characteristics, VSWR, and gain if the wearable antenna radiates toward the phantom mixture. The dielectric constant and conductivity of the phantom mixture alter the wearable antenna's electric characteristics. In this case, the antenna's resonant frequency was shifted to around 5%. However, if the wearable antenna radiates outside the phantom mixture, the antenna's VSWR and radiation pattern are almost not affected by the phantom's electrical characteristics. The sensors and antennae presented in this paper radiate outside the phantom. However, the antennas may be used in medical systems that radiate toward the human body. In this case, the antenna's resonant frequency may be shifted by around 5%, as presented in [2–4]. Comprehensive analysis and measurement setups of wearable metamaterial and fractal antennas are discussed in [2–4,52].

$$\gamma = \sqrt{j\varpi\mu(\sigma + j\omega\varepsilon)} = \alpha + j\beta \tag{8}$$

$$\alpha = Re(\gamma) \tag{9}$$

Electromagnetic waves propagating in free space can be harvested by the meta-fractal antennas and converted to DC power that may recharge the healthcare system batteries, wearable devices, and other wearable 5G and IoT devices. Energy-harvesting units are discussed and presented in [45–49]. Reference [50] highlights the significance of wearable sensors and IoT devices.

Reference [50] presents a survey about the advanced solutions and technologies that can help IoT-enabled smart grids and blockchain devices to be more resilient and secure in overcoming existing cyber and physical attacks. In this regard, in the future, the broad implementation of cutting-edge secure and data transmission systems based on block-chain techniques is necessary to safeguard the entire electrical grid against cyber-physical adversaries. Wearable sensors and antennas can be employed in smart grids and medical applications; see [51,52]. A smart grid integrates computer, communication, and sensing technologies into existing power grid networks to achieve significant informatization-related advantages. A smart grid may provide communication between neighbors, localized management, as well as bidirectional power transfer, and effective demand responses.

The antennas and sensors S_{11} and S_{21} parameter measurements were conducted by using a two-port calibrated network analyzer, as shown in Figure 21. The sensor's gain is obtained by measuring S_{21}. The two-port S parameter measurement setup is shown in Figure 21. The fabricated stacked fractal antenna structure is shown in Figure 22a. The ground plane of the fabricated stacked fractal antenna is shown in Figure 22a. The active and passive antennas presented in this paper are part of the communication systems that transmit short pulses. The absorption rate—the SAR in these cases—is low. Moreover, SAR computation is important for transmitting systems. The transmitted power of the sensors presented in this paper is lower than 20 dBm. This power rate was approved by the FDA—the Food and Drug Association—for communication devices.

(**a**)　　　　　　　　　　　　　　　　　(**b**)
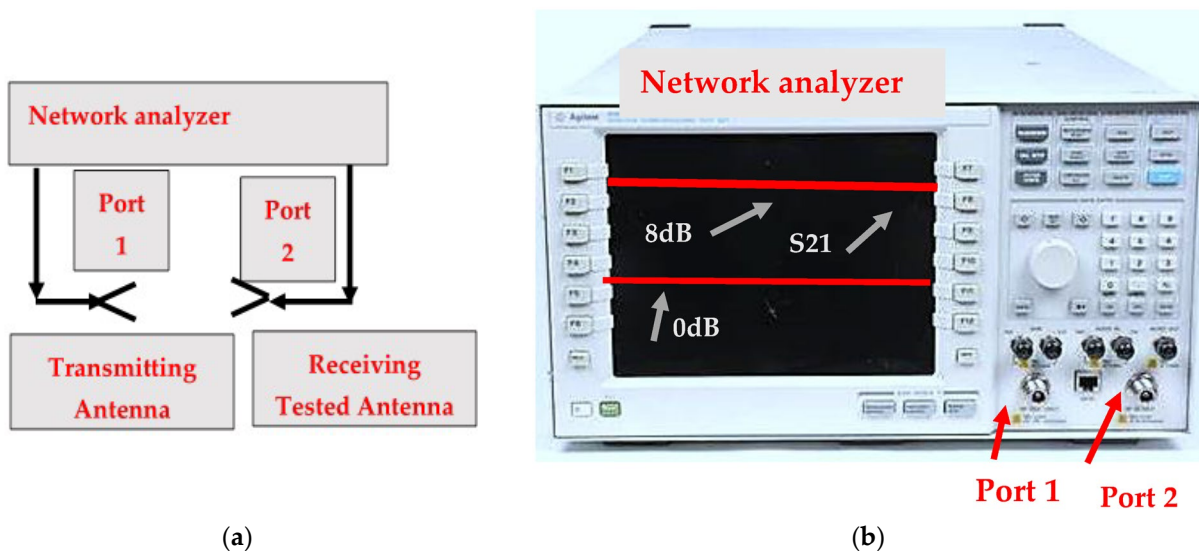
Figure 21. (**a**) Gain measurements. (**b**) Network analyzer S_{21} measurements.
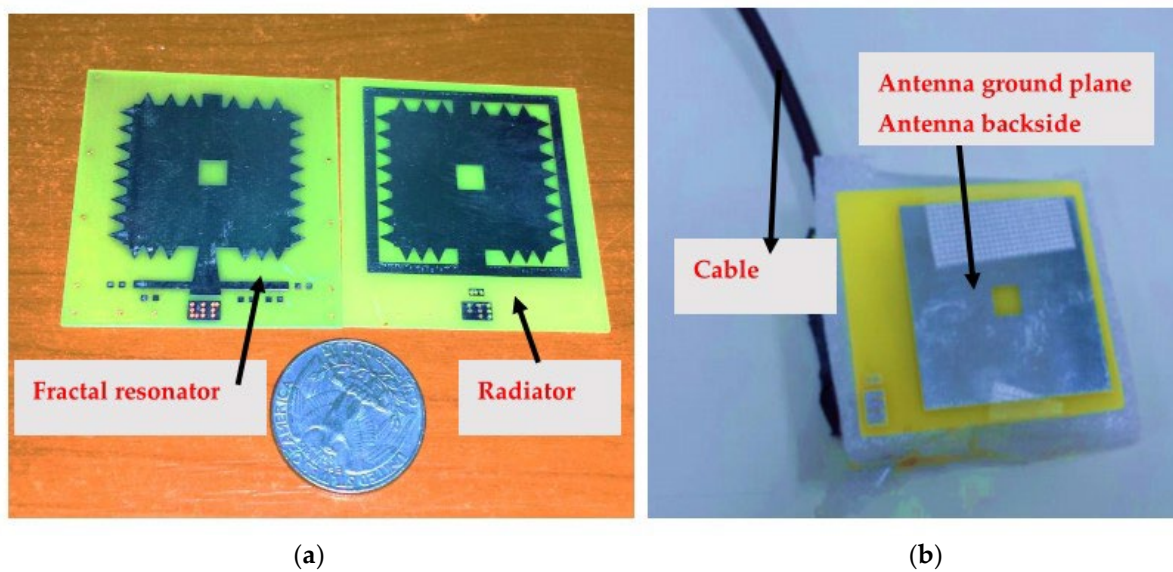
Figure 22. (**a**) The fabricated fractal-stacked antenna structure. (**b**) Antenna backside.

10. Conclusions

New green linear and dual-polarized metamaterial sensors and antennas for 5G, medical devices, Internet of Things (IoT) systems, the smart grid, and healthcare monitoring devices are presented in this paper. The active and passive metamaterial fractal antennas and sensors discussed in this article are compact, multiband, wideband, efficient, and low-cost. Energy-harvesting units can be connected to the sensors presented in this paper to provide green, renewable energy and may eliminate the usage of power cords and the need to replace batteries frequently. The development of passive and active metamaterial wearable sensors and antennas that are fractal, compact, and efficient is crucial in the evaluation of medical devices, 5G, 6G, IoT, and healthcare monitoring devices. The metamaterial fractal dual- and circular-polarized antennas and sensors presented in this paper can be used in wideband wearable RF devices for the IoT, 5G, 6G, smart grid, and medical systems. In the receiving meta-fractal antenna, a PHEMT LNA TAV541 is connected to the antenna feed line via a printed input-matching circuit that matches the antenna to the LNA. A printed output-matching circuit matches the LNA output to the receiver. Passive and active meta-fractal sensor performances, such as the bandwidth, noise figure, efficiency, gain, and radiation characteristics, were presented in this paper. Metamaterials and fractal technologies are used to develop compact, efficient antennas. The resonant frequency of the antennas with CSRR and fractal segments is lower by 4% to 9% than that of the antennas without CSRR and fractal segments. The directivity and gain of the antennas with CSRR and fractal segments are higher by 2 dB to 3 dB than that of the antennas without CSRR. The electrical-simulated and measured results of the compact meta-fractal antennas with and without CSRRs are presented in this paper. The small size of the antennas presented in this paper allows them to be attached to the human body. The antennas have conformal features. The fractal metamaterial antennas presented in this paper are compact with dimensions less than 0.55λ, and they can be used as radiating elements in antenna arrays.

The circular-polarized meta-fractal antenna's circularity is around 1 dB circularity. The active receiving antenna gain is around 13.5 dB at 2.83 GHz and decreases to 8 dB at 3.2 GHz, and the receiving module noise figure with the TAV541 LNA is around 1 dB. The meta-fractal antennas and sensors discussed in this paper may operate in medical systems to improve the daily life conditions and health of individuals all over the world. Wearable antennas and healthcare sensors are a significant choice for healthcare centers, medical organizations, communities, and patients. Meta-fractal wearable antennas support the

development of medical systems with immediate online physician responses to treat and improve patients' health. In future research, developers and researchers should develop healthcare monitoring systems to provide efficient and low-cost medical services.

Energy-harvesting circuits may be connected to the antennas and sensors to provide self-powered, autonomous, small, active antennas. Future medical devices and sensors should use green materials and energy.

All sensors presented in this paper were evaluated by employing RF electromagnetic software. There is a good match between the calculated and measured results.

The metamaterial sensors and antenna presented in this paper may be used in advanced applications and technologies that can help IoT-enabled smart grids and blockchain to be more resilient and secure in overcoming existing cyber and physical attacks. In the future, the broad implementation of secure, cutting-edge data transmission systems based on blockchain techniques is necessary to safeguard the entire electrical grid against cyber-physical adversaries.

In future research, we will develop wideband, wearable, compact, efficient, active receiving and transmitting sensors with efficient advanced LNAs and power amplifiers with energy-harvesting modules.

In future work, several types of fractal and metamaterial small antennas and sensors for medical, 5G, cellular phones, and IoT systems with energy-harvesting units will be evaluated and discussed. In future research, efficient linear and circular-polarized compact sensors and antennas for 5G and 6G communication systems, as well as medical, IoT, and other applications, will be developed.

Conflicts of Interest: The authors declare no conflict of interest.

References

1. Constantine, A. *Balanis, Antenna Theory Analysis and Design*, 4th ed.; Wiley Sons: Hoboken, NJ, USA, USA, 2016.
2. Sabban, A. *Novel Wearable Antennas for Communication and Medical Systems*; Taylor & Francis Group: Boca Raton, FL, USA, 2017.
3. Sabban, A. *Wideband RF Technologies and Antennas in Microwave Frequencies*; Wiley: Hoboken, NJ, USA, 2016.
4. Sabban, A. *Low Visibility Antennas for Communication Systems*; Taylor & Francis: Boca Raton, FL, USA, 2015.
5. Waher, P. *Learning Internet of Things*; Packt Publishing: Birmingham, UK, 2015; ISBN 13:97-81783553532.
6. Rajab, K.; Mittra, R.; Lanagan, M. Size Reduction of Microstrip Antennas using Metamaterials. In Proceedings of the 2005 IEEE APS Symposium, Washington, DC, USA, 3–8 July 2005.
7. Pendry, J.B.; Holden, A.J.; Stewart, W.J.; Youngs, I. Extremely Low Frequency Plasmons in Metallic Meso-structures. *Phys. Rev. Lett.* **1996**, *76*, 4773–4776. https://doi.org/10.1103/physrevlett.76.4773.
8. Pendry, J.B.; Holden, A.; Robbins, D.; Stewart, W. Magnetism from conductors and enhanced nonlinear phenomena. *IEEE Trans. Microw. Theory Tech.* **1999**, *47*, 2075–2084. https://doi.org/10.1109/22.798002.
9. Marqués, R.; Mesa, F.; Martel, J.; Medina, F. Comparative analysis of edge and broadside coupled split ring resonators for metamaterial design—Theory and Experiment. *IEEE Trans. Antennas Propag.* **2003**, *51*, 2572–2581.
10. Marqués, R.; Baena, J.D.; Martel, J.; Medina, F.; Falcone, F.; Sorolla, M.; Martin, F. Novel small resonant electromagnetic particles for metamaterial and filter design. In Proceedings of the ICEAA'03, Torino, Italy, 8–12 September 2003; pp. 439–442.
11. Marqués, R.; Martel, J.; Mesa, F.; Medina, F. Left-Handed-Media Simulation and Transmission of EM Waves in Subwavelength Split-Ring-Resonator-Loaded Metallic Waveguides. *Phys. Rev. Lett.* **2002**, *89*, 183901. https://doi.org/10.1103/physrevlett.89.183901.
12. Zhu, J.; Eleftheriades, G. A Compact Transmission-Line Metamaterial Antenna with Extended Bandwidth. *IEEE Antennas Wirel. Propag. Lett.* **2008**, *8*, 295–298. https://doi.org/10.1109/LAWP.2008.2010722.
13. Baena, J.D.; Marqués, R.; Martel, J.; Medina, F. Experimental results on metamaterial simulation using SRR-loaded Waveguides In Proceedings of the IEEE-AP/S International Symposium on Antennas and Propagation, Columbus, OH, USA, 22–27 June 2003; pp. 106–109.
14. Marques, R.; Martel, J.; Mesa, F.; Medina, F. A new 2D isotropic left-handed metamaterial design: Theory and experiment. *Microw. Opt. Technol. Lett.* **2002**, *35*, 405–408. https://doi.org/10.1002/mop.10620.
15. Sabban, A. New Compact Wearable Metamaterials Circular Patch Antennas for IoT, Medical and 5G Applications. *Appl. Syst. Innov.* **2020**, *3*, 42. https://doi.org/10.3390/asi3040042.
16. Sabban, A. Small Wearable Metamaterials Antennas for Medical Systems. *Appl. Comput. Electromagn. Soc. J.* **2016**, *31*, 434–443.

17.   Fujimoto, K. *Antenna for Small Mobile Terminals*; Artech House: Norwood, MA, USA, 2018.

18.   Sabban, A. Wearable Antenna Measurements in Vicinity of Human Body. *Wirel. Eng. Technol.* **2016**, *7*, 97–104. https://doi.org/10.4236/wet.2016.73010.

19.   Sabban, A. Active Compact Wearable Body Area Networks for Wireless Communication, Medical and IOT Applications. *Appl. Syst. Innov. J.* **2018**, *1*, 46. https://doi.org/10.3390/asi1040046.

20.   Mandelbrot, B.B. *The Fractal Geometry of Nature*; W.H. Freeman and Company: New York, NY, USA, 1983.

21.   Falkoner, F.J. *The Geometry of Fractal Sets*; Cambridge University Press: Cambridge, UK, 1990.

22.   Rusu, M.V.; Baican, R. Chapter 16–Fractal Antenna Application. In *Microwave and Millimeter Wave Technologies from Photonic Bandgap Devices to Antenna and Applications*; Minin, I., Ed.; INTECH: London, UK, 2010; pp. 351–382, ISBN 978-953-7619-66-4.

23.   Rusu, M.V.; Hirvonen, M.; Rahimi, H.; Enoksson, P.; Rusu, C.; Pesonen, N.; Vermesan, O.; Rustad, H. Minkovsky Fractal Microstrip Antenna for RFID Tags. In Proceedings of the 2008 38th European Microwave Conference, Amsterdam, The Netherlands, 27–31 October 2008.

24.   Rahimi, H.; Rusu, M.; Enoksson, P.; Sandström, D.; Rusu, C. Small Patch Antenna Based on Fractal Design for Wireless Sensors. In Proceedings of the 18th Workshop on Micromachining, Micromechanics, and Microsystems, MME07, Guimaraes, Portugal, 16–18 September 2007.

25.   Mandelbrot, B.B. How long is the coast of Britain? Statistical self-similarity and fractional dimension. *Science* **1967**, *156*, 636–638.

26.   Chirwa, L.; Hammond, P.; Roy, S.; Cumming, D.R.S. Electromagnetic radiation from ingested sources in the human intestine between 150 MHz and 1.2 GHz. *IEEE Trans. Biomed. Eng.* **2003**, *50*, 484–492. https://doi.org/10.1109/tbme.2003.809474.

27.   Werber, D.; Schwentner, A.; Biebl, E.M. Investigation of RF transmission properties of human tissues. *Adv. Radio Sci.* **2006**, *4*, 357–360. https://doi.org/10.5194/ars-4-357-2006.

28.   Gupta, B.; Sankaralingam, S.; Dhar, S. Development of wearable and implantable antennas in the last decade: A review. In Proceedings of the 2010 10th Mediterranean Microwave Symposium, Guzelyurt, Cyprus, 25–27 August 2010; pp. 251–267.

29.   Thalmann, T.; Popovic, Z.; Notaros, B.M.; Mosig, J.R. Investigation and design of a multi-band wearable antenna. In Proceedings of the 3rd European Conference on Antennas and Propagation, EuCAP 2009, Berlin, Germany, 23–27 March 2009; pp. 462–465.

30.   Salonen, P.; Rahmat-Samii, Y.; Kivikoski, M. Wearable antennas in the vicinity of human body. In Proceedings of the IEEE Antennas and Propagation Society Symposium, Monterey, CA, USA, 20–25 June 2004; pp. 467–470.

31.   Kellomäki, T.; Heikkinen, J.; Kivikoski, M. Wearable antennas for FM reception. In Proceedings of the 2006 First European Conference on Antennas and Propagation, Nice, France, 6–10 November 2006; pp. 1–6.

32.   Sabban, A. Microstrip Antenna and Antenna Arrays. U.S. Patent 4,623,893, 18 November 1986.

33.   Wheeler, H.A. Small antennas. *IEEE Trans. Antennas Propag.* **1975**, *23*, 462–469.

34.   Jamil, F.; Ahmad, S.; Iqbal, N.; Kim, D. Towards a Remote Monitoring of Patient Vital Signs Based on IoT-Based Blockchain Integrity Management Platforms in Smart Hospitals. *Sensors* **2020**, *20*, 2195. https://doi.org/10.3390/s20082195.

35.   Lin, J.; Itoh, T. Active integrated antennas. *IEEE Trans. Microw. Theory Tech.* **1994**, *42*, 2186–2194. https://doi.org/10.1109/22.339741.

36.   Mortazwi, A.; Itoh, T.; Harvey, J. *Active Antennas and Quasi-Optical Arrays*; John Wiley & Sons: New York, NY, USA, 1998.

37.   Jacobsen, S.; Klemetsen, Ø. Improved Detectability in Medical Microwave Radio-Thermometers as Obtained by Active Antennas. *IEEE Trans. Biomed. Eng.* **2008**, *55*, 2778–2785. https://doi.org/10.1109/tbme.2008.2002156.

38.   Jacobsen, S.; Klemetsen, O. Active antennas in medical microwave radiometry. *Electron. Lett.* **2007**, *43*, 606. https://doi.org/10.1049/el:20070577.

39.   Ellingson, S.W.; Simonetti, J.H.; Patterson, C.D. Design and evaluation of an active antenna for a 29–47 MHz radio telescope array. *IEEE Trans. Antennas Propag.* **2007**, *55*, 826–831.

40.   Segovia-Vargas, D.; Castro-Galan, D.; Munoz, L.E.G.; González-Posadas, V. Broadband Active Receiving Patch with Resistive Equalization. *IEEE Trans. Microw. Theory Tech.* **2008**, *56*, 56–64. https://doi.org/10.1109/TMTT.2007.912008.

41.   Rizzoli, V.; Costanzo, A.; Spadoni, P. Computer-Aided Design of Ultra-Wideband Active Antennas by Means of a New Figure of Merit. *IEEE Microw. Wirel. Compon. Lett.* **2008**, *18*, 290–292. https://doi.org/10.1109/LMWC.2008.918971.

42.   James, J.R.; Hall, P.S.; Wood, C. *Microstrip Antenna Theory and Design*; Institution of Engineering and Technology (IET): London, UK, 1981.

43.   Sabban, A. Dual Polarized Dipole Wearable Antenna. U.S. Patent 8,203,497, 19 June 2012.

44.   ADS Momentum Software, Keysightt. Available online: http://www.keysight.com/en/pc-1297113/advanced-design-system-ads?cc=IL&lc=eng (accessed on 3 January 2018).

45.   Paradiso, J.A.; Starner, T. Energy scavenging for mobile and wireless electronics. *IEEE Pervasive Comput.* **2005**, *4*, 18–27.

46.   Valenta, C.R.; Durgin, G.D. Harvesting wireless power: Survey of energy-harvester conversion efficiency in far-field, wireless power transfer systems. *IEEE Microw. Mag.* **2014**, *15*, 108–120.

47.   Nintanavongsa, P.; Muncuk, U.; Lewis, D.R.; Chowdhury, K.R. Design optimization and implementation for RF energy harvesting circuits. *IEEE J. Emerg. Sel. Top. Circuits Syst.* **2012**, *2*, 24–33.

48.   Devi, K.K.A.; Sadasivam, S.; Din, N.M.; Chakrabarthy, C.K. Design of a 377 Ω patch antenna for ambient RF energy harvesting at downlink frequency of GSM 900. In Proceedings of the 17th Asia Pacific Conference on Communications (APCC '11), Sabah, Malaysia, 2–5 October 2011; pp. 492–495.

49.   Sabban, A. Wearable Circular Polarized Antennas for Health Care, 5G, Energy Harvesting, and IoT Systems. *Electronics* **2022**, *11*, 427. https://doi.org/10.3390/electronics11030427.

50. Goudarzi, A.; Ghayoor, F.; Waseem, M.; Fahad, S.; Traore, I. A Survey on IoT-Enabled Smart Grids: Emerging, Applications, Challenges, and Outlook. *Energies* **2022**, *15*, 6984. https://doi.org/10.3390/en15196984.

51. Waseem, M.; Khan, M.A.; Goudarzi, A.; Fahad, S.; Sajjad, I.A.; Siano, P. Incorporation of Blockchain Technology for Different Smar Grid Applications: Architecture, Prospects, and Challenges. *Energies* **2023**, *16*, 820. https://doi.org/10.3390/en16020820.

52. Sabban, A. *Wearable Communication Systems and Antennas: Design, Efficiency, and Miniaturization Techniques*, 2nd ed.; IOP Publication: Bristol, UK, June 2022.

53. Chandravanshi, S.; Katare, K.K.; Akhtar, M.J. A Flexible Dual-Band Rectenna With Full Azimuth Coverage. *IEEE Access* **2021**, *9*, 27476–27484. https://doi.org/10.1109/ACCESS.2021.3058239.

54. Rao, N. Modified Sierpinski and its use in Fractal Patch Antenna for Miniaturization and Multiband, Behavior. In Proceedings of the 2022 IEEE Microwaves, Antennas, and Propagation Conference NAPCON, Bangalore, India, 12–16 December 2022. https://doi.org/10.1109/MAPCON56011.2022.10047750.

55. Shrivastava, S.; Bansal, A.; Malhotra, S. Compact wearable textile antenna design for Biomedical Applications. In Proceedings of the 2023 First International Conference on Microwave, Antenna and Communication (MAC), Prayagraj, India, 24–26 March 2023. https://doi.org/10.1109/MAC58191.2023.10177127.

56. Hong, K.-D.; Zhang, X.; Zhu, L.; Yuan, T. A High-Gain and Pattern-Reconfigurable Patch Antenna Under Operation of TM_{20} and TM_{21} Modes. *IEEE Open J. Antennas Propag.* **2021**, *2*, 646–653. https://doi.org/10.1109/OJAP.2021.3079886.

57. Suhas, D.; Bhattacharyya, S. Electrically Small Broadband CRLH Metamaterial Inspired Antenna in C band for 5G Laptop Applications. In Proceedings of the 2023 IEEE Wireless Antenna and Microwave Symposium (WAMS), Ahmedabad, India, 7–10 June 2023. https://doi.org/10.1109/WAMS57261.2023.10242879.